

Homogenization of peristaltic flows in piezoelectric porous media

E. Rohan^{a,*}, V. Lukeš^a

^aDepartment of Mechanics & NTIS New Technologies for Information Society, Faculty of Applied Sciences, University of West Bohemia in Pilsen, Univerzitní 22, 30100 Plzeň, Czech Republic

Abstract

The paper presents a two-scale model of periodic porous piezoelectric structures saturated by a Newtonian fluid. The fluid flow is propelled by peristaltic deformation of the microchannels which is induced due to locally controllable piezoelectric segments actuated by propagating voltage waves. The homogenization method is employed to derive the limit macroscopic model of a poroelastic medium with the effective parameters modified due the piezoelectric properties of the skeleton. To capture the peristaltic pumping effect, the nonlinearity associated with the deforming configuration must be respected. In the homogenized linear model, this nonlinearity is introduced by deformation-dependent homogenized coefficients of the macroscopic equations. For this, a linear expansions based on the sensitivity analysis of the homogenized coefficients with respect to the deformation induced by the macroscopic quantities is employed. This enables to avoid the two-scale tight coupling of the macro- and microproblems otherwise needed when nonlinear problems are considered. The derived model is implemented and verified using direct numerical simulations of the periodic heterogeneous medium. Numerical results demonstrate the peristaltic driven fluid propulsion in response to the electric actuation and the efficiency of the proposed treatment of the nonlinearity.

Keywords: multiscale modelling, piezoelectric material, porous media, homogenization

*Corresponding author

Email addresses: rohan@kme.zcu.cz (E. Rohan), vlukes@kme.zcu.cz (V. Lukeš)

1. Introduction

The peristaltic flow is induced by deforming wall of a channel. The study of this phenomenon is of a great importance in physiology and biomechanics [16, 3, 21, 10], however, as a driving mechanism of fluid transport, it presents an important and challenging issue in the design of smart “bio-inspired” materials. We consider locally periodic porous structures saturated by a Newtonian fluid controllable by locally distributed piezoelectric segments which can induce peristaltic deformation wave of the microchannels, in contrast with biological tissues where other physiological mechanisms, namely muscular contraction provide the desired actuation.

The intention of the paper is to contribute to newly emerging and perspective area of controllable and adaptive structures equipped with embedded actuators and sensors connected to electric circuits, which provide a higher level of multi-functionality such as the capability to harvest energy or to suppress undesired vibrations. The controllable metamaterials bring many challenging problems for the field of continuum mechanics and multiscale modelling. Besides the passive nonlinear mechanical behaviour (geometric nonlinearity due to large deformations, or displacements, or material nonlinearity due to multiphysics coupling), the nonlinearity emerges also due to the electric circuit control. Moreover, by the consequence, such metamaterials can exhibit nonlocal properties which, in a sense, break the axiom of neighbourhood. Controlling and tuning of nonlinearities arising from the fluid-structure interaction coupled in space and time, being connected with a “smart” on-line/real-time control system provides wide range of applicability in the design of robotic structures and adaptive shape morphing applications.

Effective material properties of composites involving piezoelectric components have been studied since a long time. The research of electro-mechanical transduction in porous structures [28, 30] motivated the applications in activated bio-piezo porous implants. In the context of the multiscale modelling, the design of a new type of bio-materials assisting in bone healing and regeneration processes motivated the homogenization of the periodic composites consisting of piezoelectric matrix and elastic anisotropic inclusions [18], cf. [24] where the sensitivity of the effective material properties w.r.t. the inclusion shape was developed. An asymptotic analysis has been applied to derive higher order models of piezoelectric rods and beams, starting from the 3D piezoelectricity problem [29]. Besides the classical periodic homogenization [26, 8, 7], the Suquet method of homogenization has been used

to obtain analytic models of particulate and fibrous piezoelectric composites [13]. The micromechanics approaches including the Mori-Tanaka and self consistent upscaling schemes were employed in [2]. Beyond the linear piezoelectric effect, the issue of composite materials providing an apparent flexoelectric effect, related to nonuniform deformation, has been studied using the higher order continua approaches [31, 4], cf. [17]. A theory of controlled dynamic actuation of flexoelectric membranes interacting with viscous flows was introduced in [11], a work inspired by biological systems.

Novelty and paper contribution. Up to the author knowledge, the topic of peristaltic deformation induced in a fluid-saturated composite medium in response to an electro-mechanical actuation has not been reported in the literature. The paper builds on our recent works devoted to the three main issues which are synthesised in the proposed homogenization-based model of the “smart” fluid-saturated porous media describing the peristalsis-driven flow. To account for the connected porosity, the piezo-poroelastic model [23] is extended by the Darcy flow model which is obtained by the Stokes flow homogenization. For studying the fluid-structure interaction in porous flexoelectric media under large deformation in the microstructure, the homogenization approach seems to be perspective [27, 15], but inevitably leads to very complex two-scale computations (the FE^2 approach). Therefore, under the restriction of small deformation, the nonlinearity induced by the deformation-dependent effective model parameters is introduced by virtue of the sensitivity analysis approach [22]. Due to this strategy, the two-scale model is implemented. The numerical studies demonstrate the necessity of capturing the nonlinearity such that the electro-active porous medium can generate the flow.

Paper organization. In the rest of the introduction, the fluid transport driven by the peristaltic deformation in porous structures is using a reduced 1D model of the homogenized medium. The problem of the fluid interacting with the piezoelectric solid composite at the heterogeneity level of the periodic microstructure is introduced in Section 2. The homogenization procedure is described in Section 3, where the macroscopic model is derived. It involves the homogenized coefficients expressed in terms of the so-called characteristic responses of microstructures. These are given in terms of solutions to the micro-problems. The macroscopic model nonlinearity is introduced in Section 4. For this, a perturbation analysis of the homogenized coefficients

depending on the macroscopic state variables is performed, whereby some technical details are postponed in the Appendix 6. Numerical illustrations of the two-scale modelling of the PZ-controlled porous microstructures inducing the peristalsis-driven flow are reported in Section 5. The pumping effect of the homogenized medium and the key role of the model nonlinearity are demonstrated using examples of 3D microstructures with 1D and 2D fluid channel connectivity.

Notation. We employ the following notation. Since we deal with a two-scale problem, we distinguish the “macroscopic” and “microscopic” coordinates, x and x , respectively. We use $\nabla_x = (\partial_i^x)$ and $\nabla_y = (\partial_i^y)$ when differentiation w.r.t. coordinate x and y is used, respectively, whereby $\nabla \equiv \nabla_x$. By $\mathbf{e}(\mathbf{u}) = 1/2[(\nabla \mathbf{u})^T + \nabla \mathbf{u}]$ we denote the strain of a vectorial function \mathbf{u} , where the transpose operator is indicated by the superscript T . The Lebesgue spaces of 2nd-power integrable functions on an open bounded domain $D \subset \mathbb{R}^3$ is denoted by $L^2(D)$, the Sobolev space $\mathbf{W}^{1,2}(D)$ of the square integrable vector-valued functions on D including the 1st order generalized derivative, is abbreviated by $\mathbf{H}^1(D)$. Further $\mathbf{H}_\#^1(Y)$ is the Sobolev space of vector-valued Y -periodic functions (the subscript $\#$).

1D example of the homogenized metamaterial model. Using a 1D model we can illustrate the modelling approach based on the semi-linear extension of homogenized piezo-poroelastic medium controllable by electric potential wave.

Suitable symmetric boundary conditions applied to the 3D model derived in subsequent sections lead to a reduced 1D model of the macroscopically homogeneous medium involving displacement $u = u_1$, the fluid seepage $w = w_1$, the strain $e = e_{11} = u'$ and the electric potential φ which are functions of (x, t) . We consider the 1D continuum represented by interval $X =]x_-, x_+[$; upon denoting the spatial derivative by $\partial_x(\cdot) \equiv (\cdot)'$,

$$\begin{aligned} e &\equiv e_{11} , \quad e_{ij} = 0 \quad \text{for } i, j \neq 1 , \\ \nabla p &= (p', 0, 0) , \quad \text{and } \nabla \varphi = (\varphi', 0, 0) , \\ \mathbf{u} &= (u, 0, 0) , \quad \mathbf{w} = (w, 0, 0) . \end{aligned} \tag{1}$$

Since the inertia effects are neglected in the present study, only the static permeability K is required. Thus, we avoid the convolution integral arising in the dynamic Darcy flow model involving the dynamic permeability.

Moreover, in a simple way, this quasistatic restriction enables to reduce the homogenized model represented by the following equations,

$$\begin{aligned} -\sigma' &= f, \text{ where } \sigma = Ae(u) - pB + H\varphi, \\ M\dot{p} + w' + Be(\dot{u}) &= Z\dot{\varphi}, \text{ where } w = -\tilde{K}p'. \end{aligned} \quad (2)$$

Above the “dot” denotes the time derivative. The stress σ is given by the pressure p and the potential φ due to the extended poroelastic law involving coefficients A, B and H . Further we omit the volume forces f . The permeability depends on the response due to the linear expansion formula,

$$\tilde{K}(e, p, \varphi) = K_0 + \partial_e K_0 e + \partial_p K_0 p + \partial_\varphi K_0 \varphi, \quad (3)$$

which can be obtained using the sensitivity analysis of the microstructure response; $\partial_p K_0$ is the derivative of K_0 w.r.t. the pressure and, in analogy, the differentiation w.r.t. e and φ is denoted by $\partial_e K_0$ and $\partial_\varphi K_0$, respectively. For other coefficients such expansions can be considered in analogy. The mass conservation involves the homogenized coefficients M, B and Z .

Let us define

$$\begin{aligned} C &= M + BA^{-1}B, \quad F = Z + BA^{-1}H, \\ K_p &= \partial_p K_0 + \partial_e K_0 A^{-1}B, \quad K_\varphi = \partial_\varphi K_0 - \partial_e K_0 A^{-1}H. \end{aligned} \quad (4)$$

When no volume forces and no inertia effects are considered, thus, $f = 0$ in $(2)_1$, thus $\bar{\sigma}' = 0$, the stress $\sigma(x, t) = \bar{\sigma}(t)$ in the 1D continuum. The strain can be eliminated from the mass conservation

$$e = A^{-1}(Bp - H\varphi + \bar{\sigma}). \quad (5)$$

Consequently, this enables to rewrite the expansion of permeability \tilde{K} and its spatial derivative \tilde{K}' in terms of $p, \bar{\sigma}$ and φ only,

$$\tilde{K} = K_0 + \partial_e K_0 A^{-1}\bar{\sigma} + K_p p + K_\varphi \varphi, \quad \tilde{K}' = K_p p' + K_\varphi \varphi', \quad (6)$$

noting $\bar{\sigma}' = 0$. Using the Darcy law, the linear and a non-linear flow models are obtained from $(2)_2$,

$$\begin{aligned} C\dot{p} - K_0 p'' &= F\dot{\varphi}, \\ C\dot{p} - (\tilde{K}p'' + \tilde{K}'p') &= F\dot{\varphi}, \end{aligned} \quad (7)$$

where the nonlinearity arises due to the dependence of \tilde{K} and \tilde{K}' on p , as follows from (6). Upon substituting \tilde{K} and \tilde{K}' in the nonlinear flow model (7)₂ using (6), we get

$$C\dot{p} - K_0 p'' - (K_p p' + K_\varphi \varphi') p' - (\partial_e K_0 A^{-1} \bar{\sigma} + K_p p + K_\varphi \varphi) p'' = F \dot{\varphi} . \quad (8)$$

This illustrates, how the nonlinearity due to the “strain depending homogenized coefficients” emerges. We shall apply the expansion $\tilde{K}(e, p, \varphi)$ to all poroelastic coefficients, as detailed below in Section 3. The numerical results confirm the necessity to account for this kind of nonlinearity to mimic the pumping effect which enables for the fluid flow against the pressure slope. In Figs. 1 and 2, this statement is supported by a numerical example with prescribed pressures $p(x_-, t) = 0$ and $p(x_+, t) = \bar{p} = 0.1$ kPa, whereby the controlling potential $\varphi = \bar{\varphi}_0 |\sin(\omega t - kx)|$ with $\bar{\varphi}_0 = -100$ kV, $c = \omega/k = 0.8$ m/s. Solutions of (8) for the linear and nonlinear cases are illustrated in Fig. 1, in terms of the pressure $p(x, t)$ and the seepage $w(x, t)$. In Fig. 2, we depict the cumulative flux $Q_+(t)$ (at the right end) which is expressed at the endpoints x_- and x_+ for times $t > 0$ by

$$Q_\pm(t) = \pm \int_0^t w(x_\pm, \tau) d\tau , \quad (9)$$

noting that $Q_+(t) \approx Q_-(t)$ for times $t > t_0$, whereby t_0 is “large enough” to suppress effects of the initial conditions. It is readily seen that $Q(t)$ is oscillating about a constant in the linear case, indicating vanishing transport, whereas $Q(t)$ shows a linear average growth, hence the pumping effect.

2. Micromodel and the fluid-structure interaction

In the geometrical framework describing the fluid saturated porous medium at the heterogeneity level, we introduce the fluid-structure interaction problem for which the two-scale problem is obtained by the homogenization method in Section 3.

2.1. Porous piezoelectric solid saturated by static fluid

We consider a quasi-static loading of a piezoelectric skeleton interacting with a viscous fluid saturating pores in the skeleton. The piezo-poroelastic medium occupies an open bounded domain $\Omega \subset \mathbb{R}^3$ with Lipschitz boundary $\partial\Omega$. The following decomposition of Ω into the piezoelectric matrix, Ω_m^ε ,

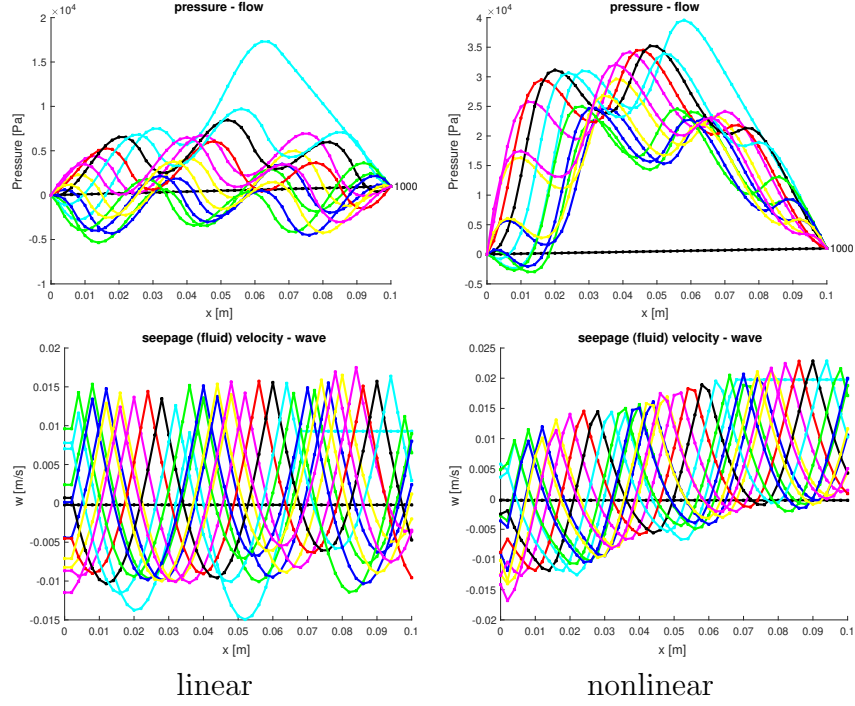


Figure 1: Spatial distributions of pressure $p(\cdot, t)$ and seepage $w(\cdot, t)$ for various time levels (the time levels specific colours: linear (left) and nonlinear (right)) models..

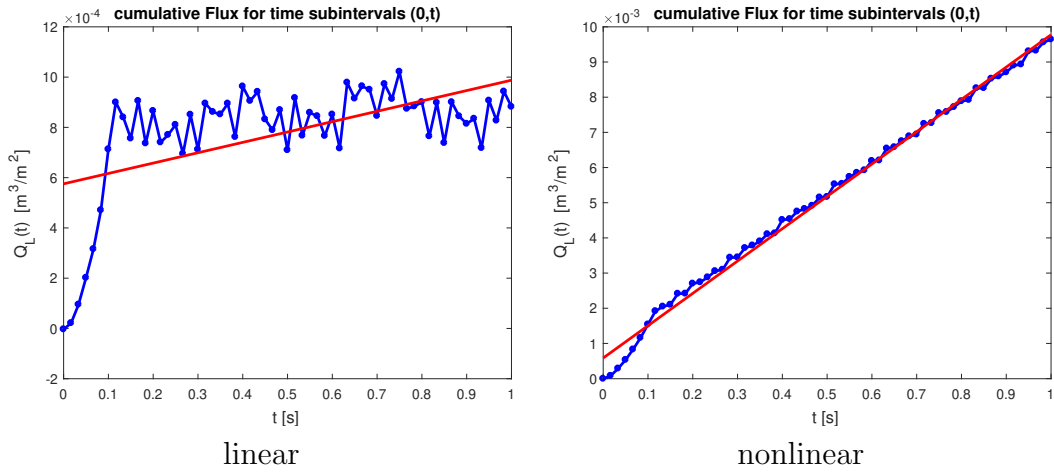


Figure 2: The cumulative fluxes $Q_+(t) [\text{m}^3/\text{m}^2]$ for the linear and nonlinear models. The regression lines show the pumping capability.

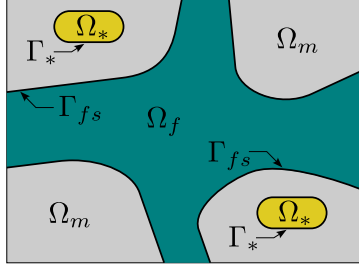


Figure 3: The representative volume element decomposition characterizing the microstructure.

elastic conductive inclusions, Ω_*^ε , and the fluid occupying the channels, Ω_f^ε , is considered:

$$\begin{aligned} \Omega &= \Omega_f^\varepsilon \cup \Omega_m^\varepsilon \cup \Omega_*^\varepsilon \cup \Gamma^\varepsilon, \quad \Omega_f^\varepsilon \cap \Omega_m^\varepsilon \cap \Omega_*^\varepsilon = \emptyset, \\ \Omega_s \equiv \Omega_{m*} &= \Omega_m^\varepsilon \cup \Omega_*^\varepsilon \cup \Gamma_*^\varepsilon, \quad \text{where } \Omega_*^\varepsilon = \bigcup_{\alpha} \Omega_*^{\alpha,\varepsilon}, \end{aligned} \quad (10)$$

where Γ^ε is the union of all interfaces separating the main three parts. Using the notation Ω_s we often refer to the solid part consisting of the piezoelectric matrix and the conductor subparts which are separated by Γ_*^ε ; this interface consists of its segments $\Gamma_*^{\alpha,\varepsilon}$ introduced, as follows:

$$\Gamma_*^\varepsilon = \bigcup_{\alpha} \Gamma_*^{\alpha,\varepsilon} \quad \text{and} \quad \Gamma_*^{\alpha,\varepsilon} = \partial\Omega_*^{\alpha,\varepsilon} \cap \overline{\Omega_m^\varepsilon}. \quad (11)$$

In (10), each $\Omega_*^{\alpha,\varepsilon}$ is assumed to be a union of segments with a diameter $\approx \varepsilon$; this restriction prevents simply connected conducting parts. Instead, these small segments are employed as the control handles allowing for a local control of the electric field due to (locally) prescribed voltage, as will be specified below. The decomposition of the microstructure is displayed in Fig. 3. By Γ_f^ε we denote the solid-fluid interface, $\Gamma_f^\varepsilon = \overline{\Omega_m^\varepsilon} \cup \overline{\Omega_*^\varepsilon} \cap \overline{\Omega_f^\varepsilon}$. The interface between the piezoelectric matrix and the conductors Γ_*^ε . Further we denote by $\partial_{\text{ext}}\Omega_m^\varepsilon = \overline{\Omega_m^\varepsilon} \cap \partial\Omega$ the exterior boundaries of Ω_m^ε . In analogy, we define $\partial_{\text{ext}}\Omega_f^\varepsilon$ as the exterior parts on the boundaries of the fluid Ω_f^ε . We assume that both the matrix Ω_m^ε and the fluid-filled channels Ω_f^ε are connected domains.

The boundary conditions for both the solid and fluid phases are prescribed on the external boundary segments $\partial_{\text{ext}}\Omega_{m*} = \partial\Omega_{m*} \cap \partial\Omega$ and $\partial_{\text{ext}}\Omega_f =$

$\partial\Omega_f \cap \partial\Omega$. The following two splits are defined, $\partial_{\text{ext}}\Omega_{m*}^\varepsilon = \Gamma_{\mathbf{u}}^\varepsilon \cup \Gamma_\sigma^\varepsilon$ and $\partial_{\text{ext}}\Omega_f^\varepsilon = \Gamma_p^\varepsilon \cup \Gamma_w^\varepsilon$ such that the “Dirichlet” type boundary conditions are prescribed on $\Gamma_{\mathbf{u}}^\varepsilon$ and Γ_p^ε , whereas the surface traction forces and fluid fluxes are prescribed on $\Gamma_\sigma^\varepsilon$ and Γ_w^ε , respectively, where

$$\Gamma_\sigma^\varepsilon = \partial_{\text{ext}}\Omega_{m*}^\varepsilon \setminus \Gamma_{\mathbf{u}}^\varepsilon, \quad \Gamma_w = \partial_{\text{ext}}\Omega_f^\varepsilon \setminus \Gamma_p^\varepsilon. \quad (12)$$

To respect spatial fluctuations of the material parameters, by virtue of the scale parameter introduced above, all material coefficients and unknown functions involved in the mathematical model which depend on the scale will be labelled by superscript ε . In the piezoelectric solid, the Cauchy stress tensor $\boldsymbol{\sigma}^\varepsilon$ and the electric displacement \vec{D}^ε depend on the strain tensor $\mathbf{e}(\mathbf{u}^\varepsilon) = (\nabla \mathbf{u}^\varepsilon + (\nabla \mathbf{u}^\varepsilon)^T)/2$ defined in terms of the displacement field $\mathbf{u}^\varepsilon = (u_i^\varepsilon)$, and on the electric field $\vec{E}(\varphi^\varepsilon) = \nabla \varphi^\varepsilon$ defined in terms of the electric potential φ^ε . The following constitutive equations characterize the piezoelectric solid in Ω_m^ε ,

$$\begin{aligned} \sigma_{ij}^\varepsilon(\mathbf{u}^\varepsilon, \varphi^\varepsilon) &= A_{ijkl}^\varepsilon e_{kl}^\varepsilon(\mathbf{u}^\varepsilon) - g_{kij}^\varepsilon E_k^\varepsilon(\varphi^\varepsilon), \\ D_k^\varepsilon(\mathbf{u}^\varepsilon, \varphi^\varepsilon) &= g_{kij}^\varepsilon e_{ij}^\varepsilon(\mathbf{u}^\varepsilon) + d_{kl}^\varepsilon E_l^\varepsilon(\varphi^\varepsilon), \end{aligned} \quad (13)$$

where $\mathbb{A}^\varepsilon = (A_{ijkl}^\varepsilon)$ is the elasticity fourth-order symmetric positive definite tensor of the solid, $A_{ijkl} = A_{klij} = A_{jilk}$. The deformation is coupled with the electric field through the 3rd order tensor $\underline{\mathbf{g}} = (g_{kij}^\varepsilon)$, $g_{kij}^\varepsilon = g_{kji}^\varepsilon$ and $\mathbf{d} = (d_{kl})$ is the permittivity tensor. The conductive solid is described by its elasticity \mathbb{A}^ε only. The permittivity in a conductor is infinitely large, so that we assume a constant potential $\varphi^\varepsilon = \bar{\varphi}^\alpha$ in any $\Omega_{*}^{\alpha,\varepsilon}$, whereby (13) reduces to the elasticity law.

In this paper we shall use a compact (global) notation, such that (13) can be written (we drop the superscript ε for the moment), $\boldsymbol{\sigma}_s = \mathbb{A}\mathbf{e}(\mathbf{u}) - \underline{\mathbf{g}}^T \cdot \vec{E}(\varphi)$, and $\vec{D} = \underline{\mathbf{g}} : \mathbf{e}(\mathbf{u}) + \mathbf{d}\vec{E}$, where $(\underline{\mathbf{g}} : \mathbf{e})_k = g_{kij}e_{ij}$. We shall not distinguish piezoelectric and dielectric (non-piezo electric) materials which both are governed by (13) with the only difference of vanishing $\underline{\mathbf{g}}$ in the latter case. In the conductor, (13)₂ is not considered.

Concerning the fluid flow described by the pressure p^ε and the velocity $\mathbf{v}^{f,\varepsilon}$ subject to the nonslip boundary conditions on the pore walls, the fluid viscosity must be scaled. We consider Newtonian fluids, such that the viscous stress rheology is given by $D_{klij}^{f,\varepsilon} = \mu^\varepsilon(\delta_{ik}\delta_{jl} + \delta_{il}\delta_{jk} - (2/3)\delta_{ij}\delta_{kl})$, where μ^ε is the dynamic viscosity. Hence the stress in fluid is given by

$$\boldsymbol{\sigma}_f^\varepsilon = -p^\varepsilon \mathbf{I} + \mathbb{D}^{f,\varepsilon} \mathbf{e}(\mathbf{v}^{f,\varepsilon}), \quad \text{where} \quad \mathbb{D}^{f,\varepsilon} = 2\mu^\varepsilon(\mathbb{I} - \frac{1}{3}\mathbf{I} \otimes \mathbf{I}). \quad (14)$$

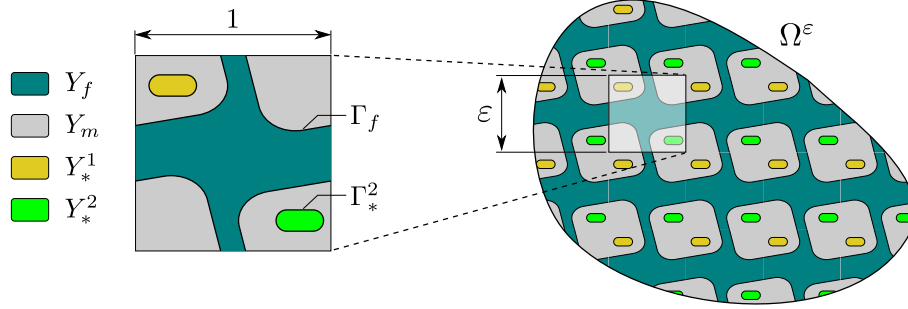


Figure 4: The scheme of the representative periodic cell decomposition and the generated periodic structure. The porous microstructure with conducting parts Y_*^α embedded in the solid piezoelectric skeleton Y_m and fluid part Y_f .

2.2. Problem formulation for the heterogeneous medium

Although in this paper we consider small deformations of the solid and the linear constitutive law (13), as will be shown, to capture the “pumping effect” of the peristaltic deformation, it is necessary to consider the nonlinearity of the fluid-structure interaction for with the interface Γ_{fs}^ϵ is associated with deforming configuration.

We shall now consider all inertia effects which are relevant to state the problem. Later on, due to restrictions to quasi-static events only, theses inertia effects will be disregarded to derive the homogenized model. The micromodel involves the following differential equations governing the fluid-solid interaction and the electric field coupled with the deformation through the piezoelectric constitutive law (13),

$$\begin{aligned}
 \rho_s \ddot{\mathbf{u}}^\epsilon - \nabla \cdot \boldsymbol{\sigma}_s^\epsilon(\mathbf{u}^\epsilon, \varphi^\epsilon) &= \mathbf{f}^{s,\epsilon}, \quad \text{in } \Omega_{m*}^\epsilon, \\
 -\nabla \cdot \vec{D}^\epsilon(\mathbf{u}^\epsilon, \varphi^\epsilon) &= q_E^\epsilon, \quad \text{in } \Omega_m^\epsilon, \\
 \mu^\epsilon \nabla^2 \mathbf{v}^{f,\epsilon} - \rho_f (\dot{\mathbf{v}}^{f,\epsilon} + \mathbf{w}^\epsilon \cdot \nabla) \mathbf{v}^{f,\epsilon} &= \nabla p^\epsilon - \mathbf{f}^{f,\epsilon}, \\
 \gamma \dot{p} + \nabla \cdot \mathbf{v}^{f,\epsilon} &= 0, \quad \text{in } \Omega_f^\epsilon,
 \end{aligned} \tag{15}$$

where γ is the fluid compressibility.

In this respect, it is convenient to use the fluid velocity decomposition

$$\mathbf{w}^\epsilon = \mathbf{v}^{f,\epsilon} - \dot{\tilde{\mathbf{u}}}^\epsilon, \tag{16}$$

where $\dot{\tilde{\mathbf{u}}}^\epsilon$ is the solid phase velocity field extended from Ω_m^ϵ to pores Ω_f^ϵ , and $\mathbf{w}^\epsilon = \mathbf{0}$ on the pore walls Γ_{fs}^ϵ .

Note that the “dot” means the material derivative. Concerning the boundary conditions, on the Neumann part of the $\partial\Omega$ partitioning, we consider prescribed traction forces $\boldsymbol{\sigma}_s^\varepsilon \cdot \mathbf{n} = \mathbf{b}^{s,\varepsilon}$ on Γ_σ , On the “Dirichlet part” of $\partial\Omega$ partitioning, the three involved fields must satisfy

$$\begin{aligned} \mathbf{u}^\varepsilon &= \mathbf{u}_\partial & \text{on } \Gamma_u^\varepsilon, \\ p^\varepsilon &= p_\partial & \text{on } \Gamma_p^\varepsilon, \\ \mathbf{v}^{f,\varepsilon} &= 0 & \text{on } \Gamma_w^\varepsilon, \\ \varphi^\varepsilon &= \bar{\varphi}_\varepsilon^\alpha, & \text{on } \Gamma_{*}^{\alpha,\varepsilon}, \alpha = 1, \dots, \bar{\alpha}. \end{aligned} \tag{17}$$

It should be noted that the control electric potential $\bar{\varphi}_\varepsilon^\alpha(t, x)$ can be defined for all $x \in \Omega$ attaining a constant value over each simply connected domain $\Omega_{*}^{\alpha,\varepsilon}$ at a given time t . We assume $\bar{\varphi}_\varepsilon^\alpha(t, \cdot) \in C^0(\Omega)$, is such that it converges strongly to some $\bar{\varphi}^\alpha(x, t)$.

The following interface conditions express the continuity of the traction stress, velocity and electric potential,

$$\begin{aligned} \mathbf{n} \cdot [\boldsymbol{\sigma}^\varepsilon] &= 0, \quad [\mathbf{u}^\varepsilon] = 0, \quad \text{on } \Gamma_*^\varepsilon, \\ \mathbf{v}^{f,\varepsilon} &= \dot{\mathbf{u}}^\varepsilon, \quad \mathbf{n} \cdot \boldsymbol{\sigma}_f^\varepsilon = \mathbf{n} \cdot \boldsymbol{\sigma}_s^\varepsilon, \text{ and } \mathbf{n} \cdot \vec{D}^\varepsilon = 0 & \text{on } \Gamma_{fs}^\varepsilon. \end{aligned} \tag{18}$$

In the weak formulations introduced below, the following admissibility sets and spaces will be employed, being defined using the boundary conditions (17),

$$\begin{aligned} \mathcal{U}^\varepsilon(\Omega_{m*}^\varepsilon) &= \{ \mathbf{v} \in \mathbf{H}^1(\Omega_{m*}^\varepsilon) \mid \mathbf{v} = \mathbf{u}_\partial \text{ on } \Gamma_u^\varepsilon \}, \\ \mathcal{V}_*(\Omega_m^\varepsilon, \{\Gamma_*^{\alpha,\varepsilon}\}_\alpha) &= \{ \varphi \in H^1(\Omega_m^\varepsilon) \mid \varphi = \bar{\varphi}_\varepsilon^\alpha \text{ on } \Gamma_*^{\alpha,\varepsilon} \}, \\ \mathcal{W}_0^\varepsilon(\Omega_f^\varepsilon) &= \{ \mathbf{v} \in \mathbf{H}^1(\Omega_f^\varepsilon) \mid \mathbf{v} = \mathbf{0} \text{ on } \Gamma_w^\varepsilon \}, \\ \mathcal{Q}^\varepsilon(\Omega_f^\varepsilon) &= \{ q \in H^1(\Omega_f^\varepsilon) \mid q = p_\partial \text{ on } \Gamma_p^\varepsilon \}, \\ \mathcal{W}_0^\varepsilon(\Omega_f^\varepsilon, \Gamma_{fs}^\varepsilon) &= \{ \mathbf{v} \in \mathbf{H}^1(\Omega_f^\varepsilon) \mid \mathbf{v} = \mathbf{0} \text{ on } \Gamma_{fs}^\varepsilon \cup \Gamma_w^\varepsilon \}, \end{aligned} \tag{19}$$

where the space $\mathcal{W}_0^\varepsilon(\Omega_f^\varepsilon, \Gamma_{fs}^\varepsilon)$ will be employed for the seepage velocity \mathbf{w}^ε . By $\mathcal{U}_0^\varepsilon(\Omega_{m*}^\varepsilon)$ and $\mathcal{Q}_0^\varepsilon(\Omega_f^\varepsilon)$ we denote the spaces associated with the affine sets $\mathcal{U}^\varepsilon(\Omega_{m*}^\varepsilon)$ and $\mathcal{Q}^\varepsilon(\Omega_f^\varepsilon)$ defined above. In analogy, $\mathcal{V}_0^\varepsilon(\Omega_m^\varepsilon, \{\Gamma_*^{\alpha,\varepsilon}\}_\alpha)$ is derived from \mathcal{V}_* by taking there $\bar{\varphi}_\varepsilon^\alpha := 0$.

2.2.1. Weak formulation (with inertia terms)

The weak formulation of (15) is obtained in a standard way, upon multiplying the respective equations by test functions and integrating by parts;

it reads: For $t > 0$, find $(\mathbf{u}^\varepsilon(t, \cdot), \varphi^\varepsilon(t, \cdot), \mathbf{v}^{f,\varepsilon}(t, \cdot), p^\varepsilon(t, \cdot)) \in \mathcal{U}^\varepsilon(\Omega_{m*}^\varepsilon) \times \mathcal{V}_*(\Omega_m^\varepsilon, \{\Gamma_*^{\alpha,\varepsilon}\}_\alpha) \times \mathcal{W}_0^\varepsilon(\Omega_f^\varepsilon) \times \mathcal{Q}^\varepsilon(\Omega_f^\varepsilon)$ such that:

$$\begin{aligned}
& \int_{\Omega_{m*}^\varepsilon} (\rho_s \ddot{\mathbf{u}}^\varepsilon \cdot \mathbf{v}^\varepsilon + \boldsymbol{\sigma}_s^\varepsilon(\mathbf{u}^\varepsilon, \varphi^\varepsilon) : \mathbf{e}(\mathbf{v}^\varepsilon)) \\
& - \int_{\Gamma_{fs}^\varepsilon} \mathbf{n}^\varepsilon \otimes \mathbf{v}^\varepsilon : \boldsymbol{\sigma}_f^\varepsilon(\mathbf{v}^{f,\varepsilon}, p^\varepsilon) = \int_{\Omega_{m*}^\varepsilon} \mathbf{f}^{s,\varepsilon} \cdot \mathbf{v}^\varepsilon + \int_{\partial_\sigma \Omega_{m*}^\varepsilon} \mathbf{b}^{s,\varepsilon} \cdot \mathbf{v}^\varepsilon, \\
& \int_{\Omega_m^\varepsilon} \vec{D}^\varepsilon(\mathbf{u}^\varepsilon, \varphi^\varepsilon) \cdot \nabla \psi^\varepsilon = \int_{\Omega_m^\varepsilon} \rho_E^\varepsilon \psi^\varepsilon, \\
& \rho_0 \int_{\Omega_f^\varepsilon} (\dot{\mathbf{v}}^{f,\varepsilon} + \mathbf{w}^\varepsilon \cdot \nabla \mathbf{v}^{f,\varepsilon}) \cdot \boldsymbol{\theta}^\varepsilon \\
& + \int_{\Omega_f^\varepsilon} \boldsymbol{\sigma}_f^\varepsilon(\mathbf{v}^{f,\varepsilon}, p^\varepsilon) : \mathbf{e}(\boldsymbol{\theta}^\varepsilon) = \int_{\Omega_f^\varepsilon} \mathbf{f}^{f,\varepsilon} \cdot \boldsymbol{\theta}^\varepsilon, \\
& \int_{\Omega_f^\varepsilon} q^\varepsilon (\gamma \dot{p}^\varepsilon + \nabla \cdot \mathbf{v}^{f,\varepsilon}) = 0, \\
& \mathbf{v}^{f,\varepsilon} = \dot{\mathbf{u}}^\varepsilon \text{ a.e. on } \Gamma_{fs}^\varepsilon,
\end{aligned} \tag{20}$$

for all test functions $(\mathbf{v}^\varepsilon, \psi^\varepsilon, \boldsymbol{\theta}^\varepsilon, q^\varepsilon) \in \mathcal{U}_0^\varepsilon(\Omega_{m*}^\varepsilon) \times \mathcal{V}_0^\varepsilon(\Omega_m^\varepsilon, \{\Gamma_*^{\alpha,\varepsilon}\}_\alpha) \times \mathcal{W}_0^\varepsilon(\Omega_f^\varepsilon) \times \mathcal{Q}_0^\varepsilon(\Omega_f^\varepsilon)$.

2.2.2. Weak formulation for the quasistatic flow (inertia effects neglected)

Further in this paper, we disregard the inertia effects, while restricting the model to describe events characterized by slow flows and deformation. By the consequence, the homogenization using the periodic unfolding method is applied to the weak formulation of the quasistatic fluid-solid interaction problem which is obtained from (20). Therein, upon substituting the constitutive relationships, the quasistatic restriction yields the following problem for $(\mathbf{u}^\varepsilon(t, \cdot), \varphi^\varepsilon(t, \cdot), \mathbf{w}^\varepsilon(t, \cdot), \bar{p}^\varepsilon(t, \cdot)) \in \mathcal{U}^\varepsilon(\Omega_{m*}^\varepsilon) \times \mathcal{V}_*(\Omega_m^\varepsilon, \{\Gamma_*^{\alpha,\varepsilon}\}_\alpha) \times$

$\mathcal{W}_0^\varepsilon(\Omega_f^\varepsilon, \Gamma_{fs}^\varepsilon) \times \mathcal{Q}(\Omega_f^\varepsilon)$ satisfying at $t > 0$

$$\begin{aligned}
& \int_{\Omega_{m*}^\varepsilon} (\mathbb{A}^\varepsilon \mathbf{e}(\mathbf{u}^\varepsilon) - \underline{\mathbf{g}}^\varepsilon \nabla \varphi^\varepsilon) : \mathbf{e}(\mathbf{v}^\varepsilon) \\
& - \int_{\Gamma_{fs}^\varepsilon} \mathbf{n}^\varepsilon \otimes \mathbf{v}^\varepsilon : \boldsymbol{\sigma}_f^\varepsilon(\mathbf{w}^\varepsilon, \dot{\mathbf{u}}^\varepsilon, p^\varepsilon) = \int_{\Omega_{m*}^\varepsilon} \mathbf{f}^{s,\varepsilon} \cdot \mathbf{v}^\varepsilon + \int_{\partial_\sigma \Omega_{m*}^\varepsilon} \mathbf{b}^{s,\varepsilon} \cdot \mathbf{v}^\varepsilon, \\
& \int_{\Omega_m^\varepsilon} ((\underline{\mathbf{g}}^\varepsilon)^T : \mathbf{e}(\mathbf{u}^\varepsilon) + \mathbf{d}^\varepsilon \nabla \varphi^\varepsilon) \cdot \nabla \psi^\varepsilon = \int_{\Omega_m^\varepsilon} \rho_E^\varepsilon \psi^\varepsilon, \\
& \int_{\Omega_f^\varepsilon} (2\mu^\varepsilon \mathbf{e}(\mathbf{w}^\varepsilon + \dot{\mathbf{u}}^\varepsilon) - p^\varepsilon \mathbf{I}) : \mathbf{e}(\boldsymbol{\theta}^\varepsilon) = \int_{\Omega_f^\varepsilon} \mathbf{f}^{f,\varepsilon} \cdot \boldsymbol{\theta}^\varepsilon, \\
& \int_{\Omega_f^\varepsilon} q^\varepsilon (\gamma \dot{p}^\varepsilon + \nabla \cdot (\mathbf{w}^\varepsilon + \dot{\mathbf{u}}^\varepsilon)) = 0,
\end{aligned} \tag{21}$$

for all $(\mathbf{v}^\varepsilon, \psi^\varepsilon, \boldsymbol{\theta}^\varepsilon, q^\varepsilon) \in \mathcal{U}_0^\varepsilon(\Omega_{m*}^\varepsilon) \times \mathcal{V}_0(\Omega_m^\varepsilon, \{\Gamma_*^{\alpha,\varepsilon}\}_\alpha) \times \mathcal{W}_0^\varepsilon(\Omega_f^\varepsilon, \Gamma_{fs}^\varepsilon) \times \mathcal{Q}_0^\varepsilon(\Omega_f^\varepsilon)$

3. Homogenization of the fluid-structure interaction problem

We build on the results obtained in [23], where disconnected porosity formed by the union of fluid-filled inclusions of size $\sim \varepsilon$ and a static, or quasi-static loading without any flow effect in these separated inclusions was considered. Even for the connected porosity allowing for the nonstationary Stokes flow, it can be shown that the homogenized parameters of the effective piezoporoelectric constitutive law can be obtained as in the static, or quasistatic case independently on the time. In [25], this property of decoupled homogenization of the solid and the fluid was obtained even in the fully dynamic case when the inertia effects are respected in terms of an acoustic linearization. This applies also in our present situation involving the piezoelectric skeleton – the homogenized flow obeys a Darcy law described in terms of a permeability tensor being computed independently of the deformation and the electric field.

3.1. Periodic geometry and the representative cell

In accordance with the decomposition (10) of domain Ω , the fluid saturated porous medium is generated by a reference periodic cell Y decomposed

into three non-overlapping subdomains Y_m , Y_f and Y_* , see Fig. 4,

$$Y = Y_m \cup Y_f \cup Y_* \cup \Gamma_Y, \quad Y_i \cap Y_j = \emptyset \text{ for } j \neq i \text{ with } i, j \in \{c, m, *\},$$

$$Y_* = \bigcup_{\alpha} Y_*^{\alpha}, \quad Y_*^{\alpha} \cap Y_*^{\alpha'} = \emptyset \text{ for } \alpha \neq \alpha', \quad Y_s \equiv Y_{m*} = Y_m \cap Y_*, \quad (22)$$

where $\text{dist}(Y_*^{\alpha}, Y_*^l) \geq s^*(1 - \delta_{kl})$ with $s^* > 0$ being the minimum distance between different conductive parts. Γ_Y , representing the union of all the interfaces, splits in two disjoint parts (in the sense of the surface measure), assuming $\partial Y_f \cap \partial Y_* = \emptyset$ (the conductors separated from the fluid)

$$\Gamma_Y = \Gamma_{fs} \cup \Gamma_{m*}, \quad \Gamma_{fs} = \overline{Y_s} \cap \overline{Y_f}, \quad \Gamma_{m*}^{\alpha} = \overline{Y_*^{\alpha}} \cap \overline{Y_m}, \quad \Gamma_{m*} = \bigcup_{\alpha} \Gamma_{m*}^{\alpha}. \quad (23)$$

We also assume well separated conductor parts, *i.e.* $\overline{Y_*^{\alpha}} \cap \partial Y = \emptyset$, such that the periodic lattice Ω_*^{α} is constituted by mutually disconnected inclusions with the perimeter $\approx \varepsilon$.

3.2. Material parameters and scaling

Specific features of the micromodel can be retained in the limit $\varepsilon \rightarrow 0$, if some of the involved material parameters are considered to depend on ε . To allow for microstructures with strongly controlled electric field, in formulation (21), potentials $\bar{\varphi}^{\alpha}$ are given for each simply connected domain $\Omega_*^{\alpha, \varepsilon}$ occupied by the perfect conductor and represented by Y_*^{α} within the cell Y . The following assumptions are made:

- a) Strongly controlled field: $\bar{\varphi}^{\varepsilon} = \bar{\varphi}^{\alpha}$ in $\Omega_*^{\alpha, \varepsilon}$,
- b) Weakly piezoelectric material: $\underline{g}^{\varepsilon} = \varepsilon \underline{\bar{g}}$, $\underline{d}^{\varepsilon} = \varepsilon^2 \underline{\bar{d}}$ in Ω_m^{ε} ,
- c) Nonslip condition on pore walls: $\underline{\mu}^{\varepsilon} = \varepsilon^2 \underline{\bar{\mu}}$ in Ω_f^{ε} .

Consistently with the assumption **a)**, since $\bar{\varphi}^{\alpha}$ does not vanish with $\varepsilon \rightarrow 0$, steep gradients on the electric potential are assumed for small ε , which must be compensated by the scaling **b)**. In the fluid part, the scaling **c)** of the viscosity by factor ε^2 is coherent with the quasistatic flow model with the nonslip conditions for the fluid velocity at Γ_f^{ε} , see *e.g.* [1, 12, 9]. This holds for problem (21), when the advection acceleration can be neglected. However, if fluid inertia is concerned, $\mu^{\varepsilon} = \varepsilon^{\beta} \bar{\mu}$ with a constant $\bar{\mu} > 0$, whereby exponent $\beta > 0$ is to be determined, cf. [5, 20].

3.3. Asymptotic expansions

The following truncated expansions (the so-called recovery sequences) of displacements, electric potential, pressure and the fluid seepage velocity can be introduced formally such that the limit equations can be derived:

$$\begin{aligned}
\mathcal{T}_\varepsilon(\mathbf{u}^\varepsilon) &\approx \mathbf{u}^{R\varepsilon}(x, y) := \mathbf{u}^{0\varepsilon}(x) + \varepsilon \mathbf{u}^{1\varepsilon}(x, y) , \\
\mathcal{T}_\varepsilon(\varphi^\varepsilon) &\approx \varphi^{R\varepsilon}(x, y) := \hat{\varphi}^{0\varepsilon}(x, y) , \\
\mathcal{T}_\varepsilon(p^\varepsilon) &\approx p^{R\varepsilon}(x, y) := p^{0\varepsilon}(x) + \varepsilon p^{1\varepsilon}(x, y) , \\
\mathcal{T}_\varepsilon(\tilde{\mathbf{w}}^\varepsilon) &\approx \tilde{\mathbf{w}}^{R\varepsilon}(x, y) := \hat{\mathbf{w}}(x, y) .
\end{aligned} \tag{24}$$

The test functions are considered in the analogous form, thus

$$\begin{aligned}
\mathcal{T}_\varepsilon(\mathbf{v}^\varepsilon(x)) &= \mathbf{v}^0(x) + \varepsilon \mathbf{v}^1(x, y) , \\
\mathcal{T}_\varepsilon(\psi^\varepsilon) &= \hat{\psi}^{0\varepsilon}(x, y) , \\
\mathcal{T}_\varepsilon(q^\varepsilon(x)) &= q^0(x) + \varepsilon q^1(x, y) , \\
\mathcal{T}_\varepsilon(\boldsymbol{\theta}^\varepsilon(x)) &= \hat{\boldsymbol{\theta}}(x, y) .
\end{aligned} \tag{25}$$

All the two-scale functions are Y -periodic in the second variable y and for almost all $t > 0$

$$\begin{aligned}
\mathbf{u}^1(\cdot, t), \mathbf{v}^1 &\in L^2(\Omega; \mathbf{H}_\#^1(Y_s)) , \quad \mathbf{u}^0(\cdot, t) \in \mathbf{H}^1(\Omega) , \\
\hat{\mathbf{w}}(\cdot, t), \hat{\boldsymbol{\theta}} &\in L^2(\Omega; \mathbf{H}_{\#0}^1(Y_f)) , \\
p^1(\cdot, t), q^1 &\in L^2(\Omega; H_\#^1(Y_f)) , \quad p^0(\cdot, t) \in H^1(\Omega) , \\
\hat{\varphi}^0(x, \cdot, t) &\in L^2(\Omega; H_{\#0*}^1(Y_m)) + \sum_\alpha \Phi^\alpha \bar{\varphi}^\alpha(\cdot, t) ,
\end{aligned} \tag{26}$$

where

$$\begin{aligned}
\mathbf{H}_{\#0}^1(Y_f) &= \{ \mathbf{v} \in \tilde{\mathbf{H}}_\#^1(Y_f) \mid \mathbf{v} = \mathbf{0} \text{ on } \Gamma_{fs} \} , \\
H_{\#0*}^1(Y_m) &= \{ \psi \in H_\#^1(Y_m) \mid \psi = 0 \text{ on } \Gamma_* \} , \\
H_{\#0,\alpha}^1(Y_m) &= H_{\#0*}^1(Y_m) + \Phi^\alpha , \quad \Phi^\alpha = \delta_{\alpha\beta} \text{ on } \Gamma_*^\beta ,
\end{aligned} \tag{27}$$

with $\Phi^\alpha \in H_\#^1(Y_m)$ otherwise given arbitrarily. Note that the nonslip condition of $\hat{\mathbf{w}}$ on Γ_{fs} is imposed due to the space $\mathbf{H}_{\#0}^1(Y_f)$. As the result, $\int_{Y_f} \nabla_y \cdot \hat{\boldsymbol{\theta}} = 0$ for any $\hat{\boldsymbol{\theta}} \in \mathbf{H}_{\#0}^1(Y_f)$.

Further we shall employ the volume fractions $\phi_f := |Y_f|/|Y|$ and $\phi_s = 1 - \phi_f$. The notion of the surface phase fractions $\bar{\phi}_s$ and $\bar{\phi}_f$ is needed as well, being introduced by virtue of the following convergences,

$$\int_{\Gamma_\sigma^\varepsilon} \vartheta \rightarrow \int_{\partial_\sigma \Omega} \bar{\phi}_s \vartheta = \int_{\partial \Omega} \bar{\phi}_s \vartheta, \quad \int_{\Gamma_p^\varepsilon} \vartheta \rightarrow \int_{\partial_p \Omega} \bar{\phi}_f \vartheta = \int_{\partial \Omega} \bar{\phi}_f \vartheta, \quad (28)$$

for all $\vartheta \in H^1(\Omega)$, where the equalities hold due to defining $\bar{\phi}_s := 0$ on $\partial \Omega \setminus \partial_\sigma \Omega$ and $\bar{\phi}_f := 0$ on $\partial \Omega \setminus \partial_p \Omega$. This will enable to introduce the effective traction stress, see below (46).

3.4. Limit two-scale equations – Fluid response in $\Omega \times Y_f$

We recall the separability of the fluid and solid responses of the microstructure as discussed *e.g.* in [25], cf. [9, 19]. It enables to derive the limit equations of the fluid flow in the microstructure formally independently of the solid part. Obviously, the fluid and solid responses are coupled at the macroscale. We omit details on the quasistatic flow homogenization – the result can be adopted from [25] dealing the dynamic fluid-structure interaction in the porous media.

Upon substituting the asymptotic expansions (24)-(25) into (21)_{3,4}, the following limit equations are obtained,

$$\begin{aligned} & \int_{\Omega} \oint_{Y_f} \mathbb{D} \mathbf{e}_y(\hat{\mathbf{w}}) : \mathbf{e}_y(\hat{\boldsymbol{\theta}}) - \int_{\Omega} \oint_{Y_f} p^1 \nabla_y \cdot \hat{\boldsymbol{\theta}} = \int_{\Omega} (\hat{\mathbf{f}}^f + p^0 \nabla_x) \cdot \oint_{Y_f} \hat{\boldsymbol{\theta}}, \\ & \int_{\Omega} \left(\nabla_x \cdot \left(\phi_f \dot{\mathbf{u}}^0 + \oint_{Y_f} \hat{\mathbf{w}} \right) + \oint_{Y_f} \nabla_y \cdot \hat{\mathbf{u}}^1 + \gamma p^0 \right) q^0 = 0, \\ & \int_{\Omega} \oint_{Y_f} q^1 \nabla_y \cdot \hat{\mathbf{w}} = 0, \end{aligned} \quad (29)$$

for all $\hat{\boldsymbol{\theta}} \in L^2(\Omega; \mathbf{H}_{\#0}^1(Y_f))$, $q^0 \in L^1(\Omega)$ and $q^1 \in L^2(Y_2)$. Above, $\hat{\mathbf{f}}^f$ is the averaged volume force satisfying $\int_{Y_f} \mathbf{f}^f \cdot \hat{\boldsymbol{\theta}} = \hat{\mathbf{f}}^f \cdot \int_{Y_f} \hat{\boldsymbol{\theta}}$.

Now the autonomous characteristic responses (\mathbf{w}^k, π^k) , $k = 1, 2, 3$ can be defined, such that (the summation in k applies),

$$\hat{\mathbf{w}} = \mathbf{w}^k (\hat{f}_k - \partial_k^x p^0), \quad p^1 = \pi^k (\hat{f}_k - \partial_k^x p^0). \quad (30)$$

The characteristic responses $\mathbf{w}^k(y)$ are solutions of the following problem: Find $\mathbf{w}^k \in \mathbf{H}_{\#0}^1(Y_f)$ and $\pi^k \in L^2(Y_f)$, such that

$$\begin{aligned} a_f(\mathbf{w}^k, \mathbf{v}) - \langle \pi^k, \nabla_y \cdot \mathbf{v} \rangle_{Y_f} &= \langle \mathbf{1}_k, \mathbf{v} \rangle_{Y_f} , \\ \langle q, \nabla_y \cdot \mathbf{w}^k \rangle_{Y_f} &= 0 , \end{aligned} \quad (31)$$

for all $\mathbf{v} \in \mathbf{H}_{\#0}^1(Y_f)$ and $q \in L^2(Y_f)$. Using the macroscopic seepage velocity defined by

$$\phi_f \mathbf{w}^0 := \oint_{Y_f} \hat{\mathbf{w}} , \quad (32)$$

mass conservation (29)₂ yields the macroscopic flow equation,

$$\gamma \dot{p}^0 + \nabla_x \cdot [\phi_f(\mathbf{w}^0 + \dot{\mathbf{u}}^0)] + \oint_{Y_f} \nabla_y \cdot \dot{\hat{\mathbf{u}}}^1 = 0 , \quad (33)$$

where $\hat{\mathbf{u}}^1$ is to be substituted using the scale-splitting formula (37), defined below.

3.5. Limit two-scale equations – Solid response in $\Omega \times Y_s$

To obtain the limit of the solid phase equilibrium, the interaction term involving the traction of the stress in the fluid expressed in terms of the fluid velocity $\tilde{\mathbf{w}}^\varepsilon + \tilde{\mathbf{u}}^\varepsilon$ and the pressure,

$$\mathcal{I}^\varepsilon(\boldsymbol{\sigma}_f^\varepsilon, \mathbf{v}^\varepsilon) = \int_{\Gamma_{fs}^\varepsilon} \mathbf{n}^{[s]} \cdot \boldsymbol{\sigma}_f^\varepsilon \cdot \mathbf{v}^\varepsilon , \quad \text{where} \quad \boldsymbol{\sigma}_f^\varepsilon = -\tilde{p}^\varepsilon \mathbf{I} + 2\mu^\varepsilon \mathbf{e}(\tilde{\mathbf{w}}^\varepsilon + \dot{\tilde{\mathbf{u}}}^\varepsilon) . \quad (34)$$

Recall that in [23], only the disconnected inclusion were considered (no flow), so that the limit term depends naturally on p^0 . For the quasistatic flow, according to [25], the limit interaction term yields

$$\mathcal{I}^\varepsilon(\boldsymbol{\sigma}_f^\varepsilon, \mathbf{v}^\varepsilon) \rightarrow \int_{\Omega} \phi_f \left(p^0 \nabla + \hat{\mathbf{f}}^f \right) \cdot \mathbf{v}^0 - \int_{\Omega} p^0 \oint_{\Gamma_{fs}} \mathbf{v}^1 \cdot \mathbf{n}^{[s]} + \int_{\partial_p \Omega} \bar{\phi}_f \bar{\mathbf{b}}^f \cdot \mathbf{v}^0 , \quad (35)$$

where $\mathbf{v}^0 \in \mathcal{U}_0(\Omega)$, $\mathbf{v}^1(x, \cdot) \in \mathbf{H}_{\#}^1(Y_s)$, and $\bar{\phi}_f$ is the boundary porosity. Note that on Γ_p^ε , the prescribed pressure p_∂ represents the boundary traction stress acting on the fluid part. Hence, by virtue of (28) the condition prescribing the averaged traction stress $\bar{\phi}_f \bar{\mathbf{b}}^f = -\mathbf{n} p_\partial$ on $\partial_p \Omega$ emerges in (35)

due to the convergence of $\mathbf{b}^{f,\varepsilon}$ acting on Γ_p^ε . Further issues concerning the boundary conditions are discussed in Section 3.6.

The homogenization procedure explained in [23] is pursued in analogy to derive the resulting limit equations. Thus, we obtain the limit of (21) using (35). We report here separately the local and the global subproblems; the local ones are obtained for vanishing \mathbf{v}^0 , such that

$$\begin{aligned} & \int_{\Omega \times Y_s} \mathbf{e}_y(\mathbf{v}^1) : \mathbb{A}(\mathbf{e}_x(\mathbf{u}^0) + \mathbf{e}_y(\mathbf{u}^1)) - \int_{\Omega \times Y_m} \mathbf{e}_y(\mathbf{v}^1) : \underline{\mathbf{g}}^T \nabla_y \hat{\varphi}^0 \\ &= \int_{\Omega} p^0 \int_{\Gamma_f} \mathbf{v}^1 \cdot \mathbf{n}^{[c]} dS_y, \\ & \int_{\Omega \times Y_m} \nabla_y \hat{\psi}^0 \cdot [\underline{\mathbf{g}} : (\mathbf{e}_x(\mathbf{u}^0) + \mathbf{e}_y(\mathbf{u}^1)) + \bar{\mathbf{d}} \nabla_y \hat{\varphi}^0] = \int_{\Omega \times Y_m} \bar{\rho}_E \hat{\psi}^0, \end{aligned} \quad (36)$$

must hold for all $\mathbf{v}^1 \in \mathbf{L}^2(\Omega; \mathbf{H}_{\#}^1(Y_m))$ and $\hat{\psi} \in L^2(\Omega; W_{\#*}(Y_m))$. Due to the linearity, the standard scale decoupling applies by introducing the correctors functions (the characteristic responses) such that the two-scale functions can be expressed, as follows:

$$\begin{aligned} \mathbf{u}^1(x, y) &= \boldsymbol{\omega}^{ij} e_{ij}^x(\mathbf{u}^0) - p^0 \boldsymbol{\omega}^P + \boldsymbol{\omega}^P \rho_E + \sum_{\alpha} \hat{\boldsymbol{\omega}}^{\alpha} \bar{\varphi}^{\alpha}, \\ \varphi^0(x, y) &= \hat{\eta}^{ij} e_{ij}^x(\mathbf{u}^0) - p^0 \hat{\eta}^P + \hat{\eta}^P \rho_E + \sum_{\alpha} \hat{\varphi}^{\alpha} \bar{\varphi}^{\alpha}. \end{aligned} \quad (37)$$

All $\boldsymbol{\omega}$, $\hat{\eta}$ and $\hat{\varphi}$ are Y-periodic, representing the displacements in the entire solid part, $Y_{m*} = Y_m \cup Y_*$ and the electric potential in the matrix part Y_m .

3.5.1. Local characteristic responses

The characteristic microproblems of the PZ-poroelastic medium are expressed using the bilinear forms:

$$\begin{aligned} a_Y^{m*}(\mathbf{u}, \mathbf{v}) &= \int_{Y_{m*}} [\mathbb{D} \mathbf{e}_y(\mathbf{u})] : \mathbf{e}_y(\mathbf{v}) dV_y, \\ g_Y^m(\mathbf{u}, \psi) &= \int_{Y_m} g_{kij} e_{ij}^y(\mathbf{u}) \partial_k^y \psi dV_y, \\ d_Y^m(\varphi, \psi) &= \int_{Y_m} [\mathbf{d} \nabla_y \varphi] \cdot \nabla_y \psi dV_y. \end{aligned} \quad (38)$$

The local characteristic responses are solutions of the following autonomous problems (independent of the macroscopic responses):

- Find $(\boldsymbol{\omega}^{ij}, \hat{\eta}^{ij}) \in \mathbf{H}_{\#}^1(Y_{m*}) \times H_{\#0*}^1(Y_m)$ for any $i, j = 1, 2, 3$ satisfying

$$\begin{aligned} a_Y^{m*}(\boldsymbol{\omega}^{ij} + \mathbf{\Pi}^{ij}, \mathbf{v}) - g_Y^m(\mathbf{v}, \hat{\eta}^{ij}) &= 0, \quad \forall \mathbf{v} \in \mathbf{H}_{\#}^1(Y_{m*}), \\ g_Y^m(\boldsymbol{\omega}^{ij} + \mathbf{\Pi}^{ij}, \psi) + d_Y^m(\hat{\eta}^{ij}, \psi) &= 0, \quad \forall \psi \in H_{\#0*}^1(Y_m), \end{aligned} \quad (39)$$

where $\mathbf{\Pi}^{ij} = (\Pi_k^{ij})$, $i, j, k = 1, 2, 3$ with components $\Pi_k^{ij} = y_j \delta_{ik}$ represents the homogeneous displacement field due to the principal macroscopic strain modes.

- Find $(\boldsymbol{\omega}^P, \hat{\eta}^P) \in \mathbf{H}_{\#}^1(Y_{m*}) \times H_{\#0*}^1(Y_m)$ satisfying

$$\begin{aligned} a_Y^{m*}(\boldsymbol{\omega}^P, \mathbf{v}) - g_Y^m(\mathbf{v}, \hat{\eta}^P) &= - \oint_{\Gamma_c} \mathbf{v} \cdot \mathbf{n}^{[c]} dS_y, \quad \forall \mathbf{v} \in \mathbf{H}_{\#}^1(Y_m), \\ g_Y^m(\boldsymbol{\omega}^P, \psi) + d_Y^m(\hat{\eta}^P, \psi) &= 0, \quad \forall \psi \in H_{\#0*}^1(Y_m). \end{aligned} \quad (40)$$

- Find $(\boldsymbol{\omega}^\rho, \hat{\eta}^\rho) \in \mathbf{H}_{\#}^1(Y_{m*}) \times H_{\#0*}^1(Y_m)$ satisfying

$$\begin{aligned} a_Y^{m*}(\boldsymbol{\omega}^\rho, \mathbf{v}) - g_Y^m(\mathbf{v}, \hat{\eta}^\rho) &= 0, \quad \forall \mathbf{v} \in \mathbf{H}_{\#}^1(Y_m), \\ g_Y^m(\boldsymbol{\omega}^\rho, \psi) + d_Y^m(\hat{\eta}^\rho, \psi) &= \oint_{\Gamma_{mc}} \psi dS_y, \quad \forall \psi \in H_{\#0*}^1(Y_m). \end{aligned} \quad (41)$$

- Find $(\hat{\boldsymbol{\omega}}^\alpha, \hat{\varphi}^\alpha) \in \mathbf{H}_{\#}^1(Y_{m*}) \times H_{\#0,\alpha}^1(Y_m)$ satisfying, for $\alpha = 1, 2, \dots, \alpha^*$,

$$\begin{aligned} a_Y^{m*}(\hat{\boldsymbol{\omega}}^\alpha, \mathbf{v}) - g_Y^m(\mathbf{v}, \hat{\varphi}^\alpha) &= 0, \quad \forall \mathbf{v} \in \mathbf{H}_{\#}^1(Y_m), \\ g_Y^m(\hat{\boldsymbol{\omega}}^\alpha, \psi) + d_Y^m(\hat{\varphi}^\alpha, \psi) &= 0, \quad \forall \psi \in H_{\#0*}^1(Y_m). \end{aligned} \quad (42)$$

In (40), the interface integral can be rewritten using the volume integral: for any $\mathbf{v} \in \mathbf{H}_{\#}^1(Y_{m*})$,

$$\oint_{\Gamma_f} \mathbf{v} \cdot \mathbf{n}^{[c]} = - \oint_{\Gamma_f} \mathbf{v} \cdot \mathbf{n}^{[m]} = - \oint_{Y_{m*}} \nabla_y \cdot \mathbf{v}. \quad (43)$$

3.6. Macroscopic problem – linear model of quasistatic flow and deformation

At the macroscopic level, the pore flow is coupled with the solid deformation in terms of the macroscopic quasistatic equilibrium arising from the solid part, and the mass conservation arising from the fluid part. The macroscopic state of the piezo-poroelastic medium is given by the couple (\mathbf{u}^0, p^0)

whereas the macroscopic electric potentials $\{\bar{\varphi}^\alpha\}$ are involved as the space-time control fields. We introduce the admissibility sets,

$$\begin{aligned}\mathcal{U}(\Omega) &= \{\mathbf{u} \in \mathbf{H}^1(\Omega) \mid \mathbf{u} = \mathbf{u}_\partial \text{ on } \partial_u \Omega\} , \\ \mathcal{Q}(\Omega) &= \{p \in H^1(\Omega) \mid p = p_\partial \text{ on } \partial_p \Omega\} .\end{aligned}\tag{44}$$

Further we employ the test function spaces $\mathcal{U}_0(\Omega)$ and $\mathcal{Q}_0(\Omega)$, associated with $\mathcal{U}(\Omega)$ and $\mathcal{Q}(\Omega)$, respectively, by virtue of prescribing the zero Dirichlet boundary conditions.

The limit boundary conditions of the Neumann type must be specified. For the solid phase, the traction stress is acting on $\Gamma_\sigma^\varepsilon$ represented by $\partial_\sigma \Omega$ in the limit. The prescribed fluid pressure on Γ_p^ε presents the Dirichlet-type boundary conditions, however, in the limit model, it acts also as the traction stress $-\mathbf{n}p_\partial$ in the macroscopic equilibrium equation for the mixture.

3.6.1. Homogenized coefficients of the PZ-poroelastic medium

We first recall the limit equations (33) and (32) arising from the flow subproblem. Substituting (30) in (33) yields the hydraulic permeability $\mathbf{K} = (K_{ij})$,

$$K_{ij} = \oint_{Y_f} w_i^j , \quad K_{ij} = K_{ji} .\tag{45}$$

Its symmetry and positive semidefiniteness follows by (31) upon substituting there $\mathbf{v} := \mathbf{w}^j$. Recall that the rank deficiency of K_{ij} appears if the porosity is not a simply connected domain.

The quasistatic equilibrium equation is obtained in the standard way due to the limit interaction integral (35) yielding the traction vector $\bar{\phi}_f \bar{\mathbf{b}}^f$ on $\partial_p \Omega$. In general, the effective volume and traction forces are involved,

$$\widehat{\mathbf{f}} = \phi_s \widehat{\mathbf{f}}^s + \phi_f \widehat{\mathbf{f}}^f , \quad \widehat{\mathbf{b}} = \bar{\phi}_s \bar{\mathbf{b}}^s + \bar{\phi}_f \bar{\mathbf{b}}^f , \quad \phi_d \widehat{\mathbf{f}}^d = \oint_{Y_d} \mathbf{f}^d , \quad d = s, f ,\tag{46}$$

where $\widehat{\mathbf{f}}^d$ are the average volume forces. The effective traction stress $\widehat{\mathbf{b}}$ is defined in terms of surface fractions $\bar{\phi}_d$, $d = f, s$ of the two phases and using the mean traction stresses $\bar{\mathbf{b}}^f$ and $\bar{\mathbf{b}}^s$ loading the fluid and solid, respectively.

Macroscopic functions $\mathbf{u}^0 \in \mathcal{U}(\Omega)$ and $p^0 \in L^2(\Omega)$ satisfy

$$\begin{aligned} & \int_{\Omega} e_{ij}^x(\mathbf{v}^0) [a_Y^{m*}(\mathbf{u}^1 - \Pi^{kl} e_{kl}^x(\mathbf{u}^0), \Pi^{ij}) - g_Y^m(\Pi^{ij}, \hat{\varphi}^0)] \\ & - \int_{\Omega} p^0 \phi_f \nabla_x \cdot \mathbf{v}^0 = \int_{\Omega} \hat{\mathbf{f}} \cdot \mathbf{v}^0 + \int_{\partial\Omega} \hat{\mathbf{b}} \cdot \mathbf{v}^0 \, dS_x, \end{aligned} \quad (47)$$

and the fluid mass conservation, see (33),

$$\int_{\Omega} q^0 \left(\phi_f \nabla_x \cdot \mathbf{u}^0 - \oint_{\Gamma_f} \mathbf{u}^1 \cdot \mathbf{n}^{[m*]} \, dS_y \right) + \int_{\Omega} \phi_f \nabla_x \cdot \mathbf{w}^0 + \gamma \int_{\Omega} \phi_f p^0 q^0 = 0, \quad (48)$$

for all $(\mathbf{v}^0, q^0) \in \mathcal{U}_0(\Omega) \times \mathcal{Q}_0(\Omega)$. It should be noted that, the electric charge conservation is satisfied at the microlevel. In (47) and (48), the two-scale functions are substituted using the split (37). Upon collecting the terms matching different macroscopic function, the expressions for the homogenized coefficients are identified, see [23],

$$\begin{aligned} A_{kl ij} &= a_Y^{m*}(\boldsymbol{\omega}^{ij} + \Pi^{ij}, \boldsymbol{\omega}^{kl} + \Pi^{kl}) + d_Y^m(\hat{\eta}^{kl}, \hat{\eta}^{ij}), \\ B_{ij} &= a_Y^{m*}(\boldsymbol{\omega}^P, \Pi^{ij}) - g_Y^m(\Pi^{ij}, \hat{\eta}^P) + \phi_f \delta_{ij} = - \oint_{Y_m} \nabla_y \cdot \boldsymbol{\omega}^{ij} + \phi_f \delta_{ij}, \\ M &= a_Y^{m*}(\boldsymbol{\omega}^P, \boldsymbol{\omega}^P) + d_Y^m(\hat{\eta}^P, \hat{\eta}^P) + \phi_f \gamma, \\ H_{ij}^{\alpha} &= a_Y^{m*}(\hat{\boldsymbol{\omega}}^{\alpha}, \Pi^{ij}) - g_Y^m(\Pi^{ij}, \hat{\varphi}^{\alpha}), \\ S_{ij} &= a_Y^{m*}(\boldsymbol{\omega}^{\rho}, \Pi^{ij}) - g_Y^m(\Pi^{ij}, \hat{\eta}^{\rho}), \\ R &= - \oint_{\Gamma_c} \boldsymbol{\omega}^{\rho} \cdot \mathbf{n}^{[c]} \, dS_y, \\ Z^{\alpha} &= - \oint_{\Gamma_f} \hat{\boldsymbol{\omega}}^{\alpha} \cdot \mathbf{n}^{[c]} \, dS_y. \end{aligned} \quad (49)$$

Above the symmetric expressions were derived using the equations of the characteristic problems (39)-(42). Clearly, $A_{kl ij} = A_{ijkl} = A_{kl ji}$, $B_{ij} = B_{ji}$, as expected for the Biot-type continuum and also $S_{ij} = S_{ji}$, $H_{ij}^{\alpha} = H_{ji}^{\alpha}$. We shall employ the “boldface” notation $\mathbb{A} = (A_{ijkl})$, $\mathbf{B} = (B_{ij})$, $\mathbf{S} = (S_{ij})$ and $\mathbf{K} = (K_{ij})$, whereas $\underline{\mathbf{H}} = (H_{ij}^{\alpha})$ and $\underline{\mathbf{Z}} = (Z^{\alpha})$ matches with $\underline{\varphi} = (\bar{\varphi}^{\alpha})$, so that $\sum_{\alpha} \mathbf{H}^{\alpha} \bar{\varphi}^{\alpha} = \underline{\mathbf{H}} \cdot \underline{\varphi}$.

3.6.2. Macroscopic problem – linear model of coupled flow and deformation

The limit macroscopic equations are obtained from the two-scale limit equations with the only non-vanishing macroscopic test functions \mathbf{v}^0 and q^0 . The weak formulation reads: For any time $t > 0$, find a couple $(\mathbf{u}^0(t, \cdot), p^0(t, \cdot)) \in \mathbf{U}(\Omega) \times P(\Omega)$ which satisfies

$$\begin{aligned} \int_{\Omega} (\mathbb{A} \mathbf{e}(\mathbf{u}^0) - p^0 \mathbf{B} + \underline{\mathbf{H}} \cdot \underline{\varphi}^0) : \mathbf{e}(\mathbf{v}^0) &= \int_{\Omega} \hat{\mathbf{f}} \cdot \mathbf{v}^0 + \int_{\partial\Omega} \hat{\mathbf{b}} \cdot \mathbf{v}^0 \, dS_x, \quad \forall \mathbf{v}^0 \in \mathcal{U}_0(\Omega), \\ \int_{\Omega} q^0 \left(\mathbf{B} : \mathbf{e}(\dot{\mathbf{u}}^0) + \dot{p}^0 M - \underline{\mathbf{Z}} \cdot \underline{\dot{\varphi}}^0 \right) &+ \int_{\Omega} \frac{\mathbf{K}}{\bar{\mu}} \left(\nabla_x p - \hat{\mathbf{f}}^f \right) \cdot \nabla_x q^0 = 0, \quad \forall q^0 \in \mathcal{Q}_0(\Omega). \end{aligned} \quad (50)$$

Upon integrating by parts in (50), the following system of equations governing the fluid flow in deforming PZ-poroelastic medium in domain $\Omega \subset \mathbb{R}^3$ is obtained,

$$\begin{aligned} -\nabla \cdot \boldsymbol{\sigma}^H(\mathbf{u}^0, p^0) &= \hat{\mathbf{f}}, \quad \text{in } \Omega, \\ \text{where } \boldsymbol{\sigma}^H(\mathbf{u}^0, p^0) &= \mathbb{A} \mathbf{e}(\mathbf{u}^0) - p^0 \mathbf{B} + \sum_{\alpha} \mathbf{H}^{\alpha} \bar{\varphi}^{\alpha} + \mathbf{S} \rho_E, \end{aligned} \quad (51)$$

and

$$\begin{aligned} \mathbf{B} : \mathbf{e}(\dot{\mathbf{u}}^0) + M \dot{p}^0 + \nabla \cdot \mathbf{w}^0 &= \sum_{\alpha} Z^{\alpha} \dot{\bar{\varphi}}^{\alpha} + R \dot{\rho}_E, \\ \text{where } \mathbf{w}^0 &= -\frac{1}{\bar{\mu}} \mathbf{K} (\nabla p^0 - \mathbf{f}^f). \end{aligned} \quad (52)$$

In the numerical examples reported in Section 5, $\rho_E \equiv 0$, as well as the volume forces are not considered.

We shall employ boundary conditions prescribed on $\partial\Omega$ being decomposed into disjoint parts Γ_i , $i = 0, 1, 2$, such that $\partial\Omega = \Gamma_0 \cup \Gamma_1 \cup \Gamma_2$. Without loss of generality, we consider $p_{\partial} = \bar{P}^i$ on Γ_i , $i = 1, 2$, and $\mathbf{u}_{\partial} = \mathbf{0}$ on $\Gamma_u \equiv \Gamma_1$

$$\begin{aligned} p^0 &= \bar{P}_i \text{ on } \Gamma_i, i = 1, 2, \\ \mathbf{n} \cdot \mathbf{w}^0 &= 0 \text{ on } \Gamma_0, \\ \mathbf{u}^0 &= \mathbf{0} \text{ on } \Gamma_1, \\ \mathbf{n} \cdot \boldsymbol{\sigma}^H &= \mathbf{0} \text{ on } \Gamma_0, \\ \mathbf{n} \cdot \boldsymbol{\sigma}^H &= -\bar{P}_2 \mathbf{n} \text{ on } \Gamma_2. \end{aligned} \quad (53)$$

Problem formulation. Let us assume zero initial conditions, vanishing (\mathbf{u}^0, p^0) at $t = 0$ in Ω corresponding to unloaded initial configuration. For given $P^k(t)$ functions of $t > 0$, whereby $P^k(0) = 0$ for $k = 1, 2$ and given electric actuation by voltages $\{\bar{\varphi}^\alpha(t, x)\}_\alpha$ defined for $(t, x) \in [0, T] \times \Omega$, with $T > 0$, whereby $\bar{\varphi}^\alpha(0, \cdot) = 0$ in Ω , find a solution $(\mathbf{u}^0, p^0)(t, x)$ satisfying (51), (52) and (53).

4. Modified formulation for nonlinear response

Although the homogenized model (51)-(52) was derived for a fixed reference configuration, it can be modified to capture some nonlinear effects which are important to simulate the peristalsis-driven flow. We adhere the approach suggested in [22] which enables to approximate the deformation-dependent homogenized coefficients. For simplicity

To lighten the notation in this section, we drop the superscript $(\cdot)^0$, which was previously used to denote macroscopic quantities.

4.1. Approximation of deformation-dependent homogenized coefficients

The approximation is based on the 1st order Taylor expansion which uses the sensitivity of homogenized coefficients w.r.t. the macroscopic variables. We shall consider all tensors and vectors labelled by $\tilde{\cdot}$ to be defined in the perturbed microconfiguration $\tilde{\mathcal{M}}(\tilde{\mathbf{u}}(x, \cdot), Y)$ which is characterized by the deformed “local” representative periodic cell $\tilde{Y}(x) = Y + \{\tilde{\mathbf{u}}(x, Y)\}$ for $x \in \Omega$. By $\tilde{\mathbf{u}}$ we refer to the displacement field reconstructed in the microstructures,

$$\tilde{\mathbf{u}}(x, y) = \mathbf{\Pi}^{ij}(y)e_{ij}^x(\mathbf{u}(x)) + \mathbf{u}^1(x, y), \quad (54)$$

where $\mathbf{u}^1(x, y)$ is defined in (37). Since $\tilde{Y}(x)$ depends on the macroscopic coordinate, the microstructure is perturbed from its periodic structure. However, the homogenization procedure can still be applied and the homogenized coefficients denoted by $\mathbb{H}(\tilde{\mathcal{M}}(\tilde{\mathbf{u}}, Y))$, in a generic sense, can be computed for the perturbed geometry which is determined by the field $\tilde{\mathbf{u}}$. Due to the sensitivity analysis, as explained in [22] and presented below, and by virtue of the split formulae (37), the perturbed coefficients $\mathbb{H}(\tilde{\mathcal{M}}(\tilde{\mathbf{u}}, Y)) \approx \tilde{\mathbb{H}}(\mathbf{e}(\mathbf{u}), p, \{\bar{\varphi}^\alpha\})$ can be approximated using the first order expansion for-

mulae which have the generic form

$$\begin{aligned}
\tilde{\mathbb{H}}(\mathbf{e}(\mathbf{u}), p, \{\bar{\varphi}^\alpha\}_\alpha) &= \mathbb{H}^0 + \delta_e \mathbb{H}^0 : \mathbf{e}(\mathbf{u}) + \delta_p \mathbb{H}^0 p + \sum_\alpha \delta_{\varphi, \alpha} \mathbb{H}^0 \bar{\varphi}^\alpha, \\
(\delta_e \mathbb{H}^0)_{ij} &:= (\partial_e (\delta \mathbb{H}^0 \circ \tilde{\mathbf{u}}))_{ij} = \delta \mathbb{H}^0 \circ (\boldsymbol{\omega}^{ij} + \boldsymbol{\Pi}^{ij}), \\
\delta_p \mathbb{H}^0 &:= \partial_p (\delta \mathbb{H}^0 \circ \tilde{\mathbf{u}}) = \delta \mathbb{H}^0 \circ (-\boldsymbol{\omega}^P), \\
\delta_{\varphi, \alpha} \mathbb{H}^0 &:= \partial_{\varphi, \alpha} (\delta \mathbb{H}^0 \circ \tilde{\mathbf{u}}) = \delta \mathbb{H}^0 \circ \hat{\boldsymbol{\omega}}^\alpha.
\end{aligned} \tag{55}$$

Coefficients \mathbb{H}^0 are computed using (49) and (45) for the reference “initial” configuration $\mathcal{M}(Y)$ and $\delta \mathbb{H}^0$ are sensitivities which are derived in Appendix 6 using the “design velocity field” method according to the shape sensitivity terminology. Thus, for any \mathbb{H} we can obtain a sensitivity expression $\delta \mathbb{H}(\vec{\mathcal{V}}) = \delta \mathbb{H} \circ \vec{\mathcal{V}}$ which is linear in the vector field $\vec{\mathcal{V}}$, such that for perturbed microconfiguration $z_i(y, \tau) = y_i + \tau \mathcal{V}_i(y)$, $y \in Y$, $i = 1, 2, 3$, $\tilde{\mathbb{H}} = \mathbb{H}^0 + \tau \delta \mathbb{H} \circ \vec{\mathcal{V}}$. Clearly, the derivatives (55) are obtained upon substituting $\vec{\mathcal{V}}$ by the specific vector field.

It should be noted, that the potentials, $\{\bar{\varphi}^\alpha(x, t)\}_\alpha$ are considered as the (given) control functions which, however, they influence directly the homogenized model parameters due to the expansion (37).

4.2. Semilinear formulation of the macroscopic problem

The variational formulation (50) can be modified to respect the deformation-dependent homogenized coefficients listed in (49) and (45) which are further referred to by \mathbb{H}^0 . For this, all \mathbb{H}^0 are substituted using $\tilde{\mathbb{H}}$, in the generic sense, as defined in (55). In the same context, by $\bar{\mathbb{H}}$ the coefficients of the linearized subproblems are denoted.

It should be stressed out, that the microproblems (39)-(42) and (31) are solved only once independently of the macroscopic problem. As well, the associated sensitivity analysis is performed for the reference non-perturbed configuration.

Semi-discretized problem. Within the time discretization with levels $t_k = k\Delta t$, $k = 0, 1, 2, \dots$ we consider two consecutive steps and the abbreviated notation $t := t_k$, $t^\triangleleft := t_{k-1}$. By $(\mathbf{u}, p) \approx (\mathbf{u}(t, \cdot), p(t, \cdot))$ we shall refer to the unknown fields at time $t = t_k \in \{t_i\}_i$, whereas $(\mathbf{u}^\triangleleft, p^\triangleleft) \approx (\mathbf{u}(t^\triangleleft, \cdot), p(t^\triangleleft, \cdot))$, thus being associated with time $t - \Delta t$. Using the implicit approximation $\dot{\mathbf{u}} \approx (\mathbf{u} - \mathbf{u}^\triangleleft)/\Delta t$, $\dot{p} \approx (p - p^\triangleleft)/\Delta t$ and $\dot{\varphi} \approx (\varphi - \varphi^\triangleleft)/\Delta t$,

Since the nonlinear problem is solved using a Newton-type iterative method, it is convenient to introduce the residual-based incremental formulation. Let us introduce the residual function,

$$\begin{aligned} \Psi^t((\mathbf{u}, p), \mathbb{F}; (\mathbf{v}, q)) &= \int_{\Omega} \left(\tilde{\mathbb{A}} \mathbf{e}(\mathbf{u}) - p \tilde{\mathbf{B}} + \tilde{\underline{\mathbf{H}}} \cdot \underline{\varphi} \right) : \mathbf{e}(\mathbf{v}) \\ &+ \int_{\Omega} q \left(\tilde{\mathbf{B}} : \mathbf{e}(\mathbf{u} - \mathbf{u}^{\diamond}) + (p - p^{\diamond}) \tilde{M} - \tilde{\underline{\mathbf{Z}}} \cdot (\underline{\varphi} - \underline{\varphi}^{\diamond}) \right) \\ &+ \int_{\Omega} \frac{\Delta t}{\bar{\mu}} \tilde{\mathbf{K}} \left(\nabla_x p - \hat{\mathbf{f}}^f \right) \cdot \nabla_x q - \left(\int_{\Omega} \hat{\mathbf{f}} \cdot \mathbf{v} + \int_{\partial_{\sigma} \Omega} \hat{\mathbf{b}} \cdot \mathbf{v} \, dS_x \right), \end{aligned} \quad (56)$$

evaluated at time t (hence the superscript in Ψ^t), where the “tilde” notation means the application of $\tilde{\mathbb{H}}$ in the generic sense of (55) for all the homogenized coefficients, and \mathbb{F} represents all loads, or control given in time and space domain $[0, T] \times \Omega$. In particular, \mathbb{F} comprises $\{\bar{\varphi}^{\alpha}(x, t)\}_{\alpha}$ and all the volume forces and surface tractions.

Now the time-discretized problem (50) is reformulated, as follows:

For a given solution $(\mathbf{u}^{\diamond}, p^{\diamond})$, find a couple $(\mathbf{u}, p) \in \mathcal{U}(\Omega) \times \mathcal{Q}(\Omega)$ which satisfies

$$\Psi^t((\mathbf{u}, p), \mathbb{F}; (\mathbf{v}, q)) = 0 \quad \text{for any} \quad (\mathbf{v}, q) \in \mathcal{U}_0(\Omega) \times \mathcal{Q}_0(\Omega). \quad (57)$$

It can be solved by successive iterations based on the straightforward decomposition introduced in terms of the recent approximation $(\bar{\mathbf{u}}, \bar{p})$ of the solutions $(\mathbf{u}, p) \in \mathcal{U}(\Omega) \times \mathcal{Q}(\Omega)$ and the correction $(\delta \mathbf{u}, \delta p) \in \mathcal{U}_0(\Omega) \times \mathcal{Q}_0(\Omega)$,

$$\mathbf{u} = \bar{\mathbf{u}} + \delta \mathbf{u}, \quad p = \bar{p} + \delta p. \quad (58)$$

The first order expansion in $(\delta \mathbf{u}, \delta p)$ leads to the obvious approximation

$$\begin{aligned} 0 &= \Psi^t((\mathbf{u}, p), \mathbb{F}; (\mathbf{v}, q)) \approx \Psi^t((\bar{\mathbf{u}}, \bar{p}), \bar{\mathbb{F}}; (\mathbf{v}, q)) \\ &+ \delta_{(u,p)} \Psi^t((\bar{\mathbf{u}}, \bar{p}), \bar{\mathbb{F}}; (\mathbf{v}, q)) \circ (\delta \mathbf{u}, \delta p) + \delta_{\mathbf{F}} \Psi^t((\bar{\mathbf{u}}, \bar{p}), \bar{\mathbb{F}}; (\mathbf{v}, q)) \circ \delta \mathbb{F}, \end{aligned} \quad (59)$$

to hold for any $(\mathbf{v}, q) \in \mathcal{U}(\Omega) \times \mathcal{Q}(\Omega)$, where $(\bar{\mathbf{u}}, \bar{p})$ is the recent iteration.

The total variation $\delta \Psi^t$ can be expressed in terms of tangential incremen-

tal coefficients $\bar{\mathbb{H}}$ defined below, in (63)-(64), see Section 4.3,

$$\begin{aligned}
\delta_{(\mathbf{u}, p)} \Psi^t((\bar{\mathbf{u}}, \bar{p}), \bar{\mathbb{F}}; (\mathbf{v}, q)) \circ (\delta \mathbf{u}, \delta p) &= \int_{\Omega} (\bar{\mathbb{A}} \mathbf{e}(\delta \mathbf{u}) - \delta p \bar{\mathbf{B}}) : \mathbf{e}(\mathbf{v}) \\
&- \int_{\Omega} (\partial_e \hat{\mathbf{f}} \circ \mathbf{e}(\delta \mathbf{u}) + \partial_p \hat{\mathbf{f}} \circ \delta p) \cdot \mathbf{v} - \int_{\partial\Omega} (\partial_e \hat{\mathbf{b}} \circ \mathbf{e}(\delta \mathbf{u}) + \partial_p \hat{\mathbf{b}} \circ \delta p) \cdot \mathbf{v} \\
&+ \frac{\Delta t}{\bar{\mu}} \int_{\Omega} \nabla q \cdot (\bar{\mathbf{K}} \nabla \delta p + \bar{\mathbf{G}} : \mathbf{e}(\delta \mathbf{u}) + \bar{\mathbf{Q}} \delta p) + \int_{\Omega} q (\bar{\mathbf{D}} : \mathbf{e}(\delta \mathbf{u}) + \bar{M} \delta p) .
\end{aligned} \tag{60}$$

Variation $\delta_{\mathbf{F}} \Psi^t((\bar{\mathbf{u}}, \bar{p}), \bar{\mathbb{F}}; (\mathbf{v}, q)) \circ \delta \mathbf{F}$ can be expressed in analogy, however, since \mathbb{F} is considered to be a given “control” at each time level and fixed during the iterations, *i.e.* $\delta \mathbf{F} \equiv 0$, $\delta_{\mathbf{F}} \Psi^t$ is not needed.

4.2.1. Algorithm of time increment step

Knowing the response at time $t^\triangleleft = t - \Delta t$, the one at time level t is computed by solving (57) iteratively using a modified Newton method based on the linearization due to (59) explained above. Since the boundary data, namely $p_\partial(t, \cdot)$, see (53)), can depend on time, we use the notation $\mathcal{U}^t(\Omega)$ and $\mathcal{Q}^t(\Omega)$, for the admissibility sets. For simplicity, however, we consider the split of $\partial\Omega$ independent of time, thus, we keep using $\mathcal{U}_0(\Omega)$ and $\mathcal{Q}_0(\Omega)$.

Given $(\mathbf{u}^\triangleleft, p^\triangleleft) \approx (\mathbf{u}(t^\triangleleft, \cdot), p(t^\triangleleft, \cdot))$, compute $(\mathbf{u}, p) \approx (\mathbf{u}(t, \cdot), p(t, \cdot))$:

- step 0: set the time-dependent control $\mathbb{F}^t := \mathbb{F}(t)$ comprising the electric potential $\varphi(t, \cdot)$ given in Ω and the boundary conditions, thereby $U^t(\Omega)$ and $P^t(\Omega)$ and define an approximation $(\bar{\mathbf{u}}, \bar{p}) \approx (\mathbf{u}^\triangleleft, p^\triangleleft) \in \mathcal{U}^t(\Omega) \times \mathcal{Q}^t(\Omega)$. where the perturbed homogenized coefficients $\bar{\mathbb{H}}$ (in the sense of the generic notation) are evaluated using $(\mathbf{u}^\triangleleft, p^\triangleleft)$ inserted in $(55)_1$ where \mathbb{H}^0 and the gradients $\delta_0 \mathbb{H}^0$ are given for the unperturbed microconfiguration (by off-line computing).
- step 1: use $(\bar{\mathbf{u}}, \bar{p})$ to define the perturbed homogenized coefficients $\bar{\mathbb{H}}$ and (56) to establish the residual $r(\mathbf{v}, q) := \Psi^t((\bar{\mathbf{u}}, \bar{p}), \mathbb{F}^t, (\mathbf{v}, q))$, where the test functions $(\mathbf{v}, q) \in \mathcal{U}_0(\Omega) \times \mathcal{Q}_0(\Omega)$.

If the desired tolerance $\epsilon > 0$ is achieved, *i.e.* $|r(\mathbf{v}, q)| < \epsilon \|(\mathbf{v}, q)\|$ for any $(\mathbf{v}, q) \in \mathcal{U}_0(\Omega) \times \mathcal{Q}_0(\Omega)$, put $\mathbf{u}^\triangleleft := \mathbf{u} = \bar{\mathbf{u}}$, $p^\triangleleft := p = \bar{p}$, and proceed to solving the response at the next time level $t^\triangleleft := t$. GOTO step 0.

- step 2: solve the following linear problem for $(\delta \mathbf{u}, \delta p) \in \mathcal{U}_0(\Omega) \times \mathcal{Q}_0(\Omega)$:

$$\delta_{(\mathbf{u}, p)} \Psi^t((\bar{\mathbf{u}}, \bar{p}), \mathbb{F}^t; (\mathbf{v}, q)) \circ (\delta \mathbf{u}, \delta p) = -\Psi^t((\bar{\mathbf{u}}, \bar{p}), \mathbb{F}^t; (\mathbf{v}, q)), \quad (61)$$

for any $(\mathbf{v}, q) \in \mathcal{U}_0(\Omega) \times \mathcal{Q}_0(\Omega)$, then update $\bar{\mathbf{u}} := \mathbf{u} = \bar{\mathbf{u}} + \delta \mathbf{u}$, $\bar{p} := p = \bar{p} + \delta p$, and GOTO step 1.

Comments. In the space-discretized version, the standard residual vector in the sense of the Galerkin finite element method replaces the functional $r(\cdot, \cdot)$.

4.3. Tangential incremental coefficients

The perturbations $\delta \mathbf{u}, \delta p, \delta \varphi$ employed in step 2 of the Algorithm 4.2.1, see (61), substituted in the integrals involved in Ψ^t , see (56), yield approximate linear expressions, as shown for the term related to the permeability,

$$\begin{aligned} & \int_{\Omega} \nabla q \cdot \tilde{\mathbf{K}}(\mathbf{e}(\mathbf{u}), p) \nabla p = \int_{\Omega} \nabla q \cdot (\mathbf{K}^0 + \partial_e \mathbf{K}^0 \circ \mathbf{e}(\mathbf{u}) + \partial_p \mathbf{K}^0 \circ p + \partial_{\varphi} \mathbf{K}^0 \circ \varphi) \nabla p \\ & \approx \int_{\Omega} \nabla q \cdot (\mathbf{K}^0 + \partial_e \mathbf{K}^0 \circ (\mathbf{e}(\bar{\mathbf{u}}) + \mathbf{e}(\delta \mathbf{u})) + \partial_p \mathbf{K}^0 \circ (\bar{p} + \delta p) + \partial_{\varphi} \mathbf{K}^0 \circ (\bar{\varphi} + \delta \varphi)) \nabla \bar{p} \\ & + \int_{\Omega} \nabla q \cdot (\mathbf{K}^0 + \partial_e \mathbf{K}^0 \circ \mathbf{e}(\bar{\mathbf{u}}) + \partial_p \mathbf{K}^0 \circ \bar{p} + \partial_{\varphi} \mathbf{K}^0 \circ \bar{\varphi}) \nabla \delta p, \end{aligned} \quad (62)$$

neglecting the “ $o(\delta^2)$ ” terms. In analogy, we proceed with all other integrals in (56).

In what follows we shall need some further notation employed in the linearization scheme: let $\mathbf{W} = \partial_e(\mathbf{X} : \bar{\mathbf{e}}) \circ \langle \cdot \rangle_e$, then $\mathbf{W} \delta \mathbf{e} = \partial_e(\mathbf{X} : \bar{\mathbf{e}}) \circ \delta \mathbf{e}$; in analogy, let $X = \partial_p(\mathbf{X} \bar{\mathbf{e}}) \circ \langle \cdot \rangle_p$, then $X \delta p = \partial_p(\mathbf{X} \bar{\mathbf{e}}) \circ \delta p$. Also the following abbreviations will be used:

$$\begin{aligned} \bar{\partial} \mathbb{H}^0 &= \partial_e \mathbb{H}^0 \circ \mathbf{e}(\bar{\mathbf{u}}) + \partial_p \mathbb{H}^0 \circ \bar{p} + \partial_{\varphi} \mathbb{H}^0 \circ \bar{\varphi}, \\ \bar{\partial} \mathbf{K}^0 &= \partial_e \mathbf{K}^0 \circ \mathbf{e}(\bar{\mathbf{u}}) + \partial_p \mathbf{K}^0 \circ \bar{p} + \partial_{\varphi} \mathbf{K}^0 \circ \bar{\varphi}, \end{aligned} \quad (63)$$

in the generic sense (the example shown for the permeability). With this notation in hand we can introduce coefficients $\bar{\mathbb{H}}(\bar{\mathbf{u}}, \bar{p})$ involved in (56), depending on $(\bar{\mathbf{u}}, \bar{p})$, and on the response $(\mathbf{u}^{\triangleleft}, p^{\triangleleft})$ at the previous time step t^{\triangleleft} ,

(recalling that the actual time level is $t = t^\natural + \Delta t$)

$$\begin{aligned}
\overline{\mathbb{A}}(\bar{\mathbf{u}}, \bar{p}) &= \mathbb{A}^0 + \bar{\partial} \mathbb{A}^0 + \partial_e(\mathbb{A}^0 \mathbf{e}(\bar{\mathbf{u}})) \circ \langle \cdot \rangle_e - \partial_e(\mathbf{B}^0 \bar{p}) \circ \langle \cdot \rangle_e + \partial_e \underline{\mathbf{H}} \bar{\varphi} \circ \langle \cdot \rangle_e, \\
\overline{\mathbf{B}}(\bar{\mathbf{u}}, \bar{p}) &= \mathbf{B}^0 + \bar{\partial} \mathbf{B}^0 + \partial_p(\mathbf{B}^0 \bar{p}) \circ \langle \cdot \rangle_p - \partial_p(\mathbb{A}^0 \mathbf{e}(\bar{\mathbf{u}})) \circ \langle \cdot \rangle_p - \partial_p(\underline{\mathbf{H}}^0 \bar{\varphi}) \circ \langle \cdot \rangle_p, \\
\overline{\mathbf{D}}(\bar{\mathbf{u}}, \bar{p}, \mathbf{u}^0, p^0) &= \mathbf{B}^0 + \bar{\partial} \mathbf{B}^0 + \partial_e \mathbf{B}^0 : (\mathbf{e}(\bar{\mathbf{u}}) - \mathbf{e}(\mathbf{u}^0)) \circ \langle \cdot \rangle_e \\
&\quad + \partial_e M^0(\bar{p} - p^0) \circ \langle \cdot \rangle_e - \partial_e \underline{\mathbf{Z}}^0(\bar{\varphi} - \varphi^0) \circ \langle \cdot \rangle_e, \\
\overline{\mathbf{M}}(\bar{\mathbf{u}}, \bar{p}, \mathbf{u}^0, p^0) &= M^0 + \bar{\partial} M^0 + \partial_p M^0(\bar{p} - p^0) \circ \langle \cdot \rangle_p \\
&\quad + \partial_p \mathbf{B}^0 : (\mathbf{e}(\bar{\mathbf{u}}) - \mathbf{e}(\mathbf{u}^0)) \circ \langle \cdot \rangle_p - \partial_p \underline{\mathbf{Z}}^0(\bar{\varphi} - \varphi^0) \circ \langle \cdot \rangle_p, \\
\overline{\mathbf{K}}(\bar{\mathbf{u}}, \bar{p}) &= \mathbf{K}^0 + \bar{\partial} \mathbf{K}^0, \\
\overline{\mathbf{G}} &= \partial_e \mathbf{K}^0(\nabla \bar{p} - \mathbf{f}) \circ \langle \cdot \rangle_e, \\
\overline{\mathbf{Q}} &= \partial_p \mathbf{K}^0(\nabla \bar{p} - \mathbf{f}) \circ \langle \cdot \rangle_p.
\end{aligned} \tag{64}$$

5. Numerical simulations

In this section, we present the results obtained by finite element (FE) two-scale numerical simulations of flows in piezoelectric porous structures. In order to validate the two-scale model of the homogenized medium presented in Section 3, as the “reference model” we consider the one governing responses of the heterogeneous medium. Accordingly, “the reference solutions” are computed using the *direct numerical simulations* (DNS) of the non-homogenized medium discretized on a “full” FE mesh which is generated as a periodic lattice of the “scaled” periodic unit cells $\varepsilon_0 Y$ with a given ε_0 . Both the two-scale simulations using the Homogenized model (HOM-model) and the DNS of the Reference model (REF-model) response have been implemented in the Python based finite element package *SfePy*: Simple Finite Elements in Python [6] which, in general, is well suited for solving problems with multi-scale and multi-physical features.

The evolutionary problems for both the HOM-model and the REF-model are solved using time stepping algorithms where the time derivatives are replaced by the backward finite differences. For the HOM-model, Algorithm 4.2.1 is implemented which includes the homogenized coefficients updating. For DNS with the REF-model, the reference configuration is being updated to capture the nonlinearity the deformation influence on the flow. The following spatial FE approximations using Lagrangian elements are employed in all calculations: the displacement, the electric potential, and the

fluid pressure fields are approximated using the P1 (piecewise linear) elements, while the fluid velocity is approximated using the P2 (piecewise quadratic) ones.

5.1. Two-scale computations with the HOM-model

Due to the treatment of the deformation-dependent homogenized coefficients $\tilde{\mathbf{H}}$ explained in Section 4.1, the micro-problems (39)-(42) and (31) for characteristic responses of the (nondeformed) microconfiguration $\mathcal{M}(Y)$, as well as the associated sensitivities (63)-(64) are solved independently of the macro-problem (57).

The microscopic domain Y is decomposed into several parts according to (22): compliant elastic part Y_e , piezoelectric matrix Y_z ($Y_e \cup Y_z = Y_m$), two mutually disconnected conductors Y_*^1 and Y_*^2 , and fluid part Y_f , see Figure 5. The material properties of the constituents are summarized in Table 1. Note

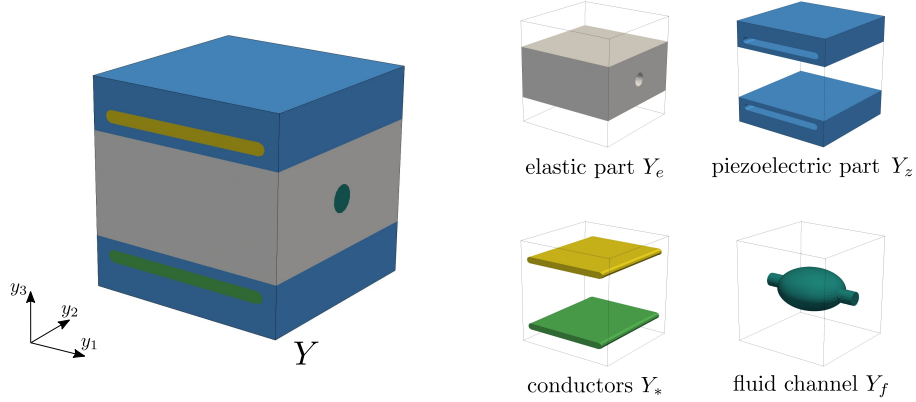


Figure 5: Decomposition of the microscopic periodic cell.

that, by virtue of the scaling introduced in Section 3.2, the characteristic responses of the microstructure are computed with the rescaled coefficients $\underline{\bar{\mathbf{g}}}$, $\underline{\bar{\mathbf{d}}}$ and $\bar{\eta}$ obtained for a given microstructure size, *i.e.* a given $\varepsilon := \varepsilon_0$.

In order to compare the HOM-model solutions with the corresponding REF-model responses obtained by the DNS we consider a “pseudo 1D problem”, such that, although Ω is a 3D block, all the macro-problem parameters, including the boundary conditions make the response of the HOM-model to depend on the x_1 coordinate only.

The macroscopic problem (51)-(52) recast for the semilinear formulation (56)-(57), is imposed in Ω represented as block with dimensions $L \times a \times$

elastic part Y_e (elastomer)	E = 0.02 GPa, $\nu = 0.49$						
piezoelectric part Y_m (piezo-polymer, [14])	$\mathbb{A} =$	$\begin{bmatrix} 6.0 & 3.72 & 3.83 & 0 & 0 & 0 \\ 3.72 & 6.0 & 3.83 & 0 & 0 & 0 \\ 3.83 & 3.83 & 20.3 & 0 & 0 & 0 \\ 0 & 0 & 0 & 1.23 & 0 & 0 \\ 0 & 0 & 0 & 0 & 1.23 & 0 \\ 0 & 0 & 0 & 0 & 0 & 1.23 \end{bmatrix}$					$\cdot 10^7 \text{ Pa}$
	$\underline{\mathbf{g}}^\varepsilon =$	$\begin{bmatrix} 0 & 0 & 0 & 0 & 0.01 & 0 \\ 0.340 & 0 & 0 & 0 & 0 & 0.01 \\ -0.09 & -0.09 & 5.91 & 0 & 0 & 0 \end{bmatrix}$					C/m ²
	$\underline{\mathbf{d}}^\varepsilon =$	$\begin{bmatrix} 18 & 0 & 0 \\ 0 & 18 & 0 \\ 0 & 0 & 255.3 \end{bmatrix}$					$\cdot 8.854 \cdot 10^{-12} \text{ C/Vm}$
conductors Y_* (steal alloy)	E = 200 GPa, $\nu = 0.25$						
fluid Y_f (water)	$\gamma = 1.0/(2.15 \cdot 10^9) \text{ Pa}$, $\eta^\varepsilon = 8.9 \cdot 10^{-4} \text{ Pa s}$						

Table 1: Material properties of the piezoelectric skeleton, Voigth representation of the strain is employed for tensors \mathbb{A} and $\underline{\mathbf{g}}^\varepsilon$. Note that $\underline{\mathbf{g}} = \underline{\mathbf{g}}^\varepsilon/\varepsilon$ and $\underline{\mathbf{d}} = \underline{\mathbf{d}}^\varepsilon/\varepsilon$ are computed for a given scale $\varepsilon := \varepsilon_0$.

Structure / flow	$\bar{\varphi}^*$ [V]	b_1	b_1	c	d
case 1D	$4 \cdot 10^5$	$\pi/0.03$	0	10π	0
case 2D	$4 \cdot 10^5$	$\pi/0.03$	$\pi/0.075$	10π	0

Table 2: Parameters of the electric potential wave, see (65).

a spanned on axes x_1, x_2 , and x_3 in the respective order. The boundary conditions, see Fig. 6, are considered according to (53), being modified on Γ_0 by periodic conditions. They are applied in the directions x_2, x_3 on all four faces with the normals alligned with either of these directions. In particular, on the faces $\Gamma_1 \equiv \Gamma_L$ and $\Gamma_2 \equiv \Gamma_R$ perpendicular to x_1 axis, we prescribe: $\mathbf{u} = \mathbf{0}$, $p = 0$ on Γ_L , whereas $p = \bar{p}$ on Γ_R , with \bar{p} [Pa] a given pressure value; this defines also the surface traction $\hat{\mathbf{b}} = -\bar{p}\mathbf{n}$. The boundary conditions are depicted in Fig. 6

While $\bar{\varphi}^1 = 0$ is prescribed on the first electroode, the potential waves propagate due to the second electrode, wherenby the electric potential φ^2 to be a function depending on time t and coordinates $x_1 \in]0, L[$ and $x_2 \in]0, a[$:

$$\begin{aligned} \psi(x_1, x_2, t) &:= b_1 x_1 + b_2 x_2 - c t + d, \\ \varphi^2(x_1, x_2, t) &= \begin{cases} \frac{1}{2} [1 + \cos(\psi(x_1, x_2, t) + \pi)] \bar{\varphi}^*, & \text{for } \psi(x_1, x_2, t) < 0 \\ 0 & \text{otherwise} \end{cases}, \end{aligned} \quad (65)$$

where b_1, b_2, c , and d are constants specified for the examples reported below as “1D” and “2D” cases, and the voltage wave amplitude $\bar{\varphi}^*$ is adjusted accordingly to the case, see Tab. 2. The above setting ensure the macroscopic displacements \mathbf{u} and the pressure gradient $\nabla_x p$ induced by the electric potential to be non-zero only in x_1 direction, thus, the “pseudo 1D problem” intentions are met. Due to the periodicity in the x_2 and x_3 directions, the length a can be arbitrary, but for a better comparison with the reference calculation due to the REF-model, we choose $a := L/N$, where N is the number of the real-sized periods $Y^{\varepsilon_0} = \varepsilon_0 Y$, see the next subsection.

5.2. Reference simulation with the REF-model

For a validation of the homogenized model and verification of its numerical implementation the approach of the direct numerical simulations (DNS)

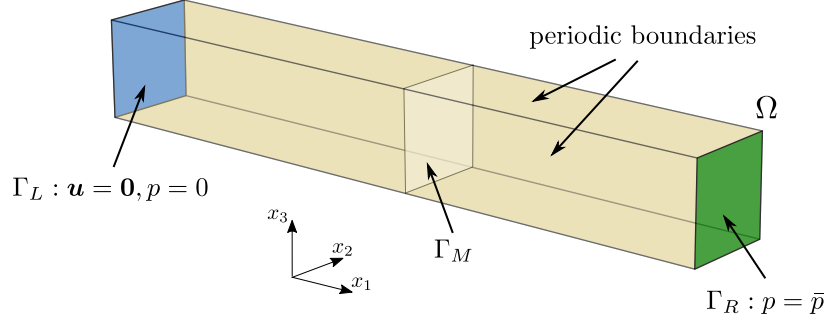


Figure 6: Macroscopic domain $\Omega =]0, L[\times]0, a[^2$ and applied boundary conditions. The positions of sections Γ_L , Γ_M , and Γ_R are $x_1 = 0, L/2$ and L , respectively.

of the heterogeneous continuum response is employed. The reference response of the REF-model is obtained as the solutions of problem (21) with the material parameters given Tab. 1. In connection with the HOM-model, we set $L = 0.1$ m and $a = L/N = 0.005$ m with $N = 20$, which yields $\varepsilon_0 = 0.005$. The general decomposition (10) holds, where in the solid phase $\Omega_s^{\varepsilon_0} = \Omega_e^{\varepsilon_0} \cup \Omega_z^{\varepsilon_0} \cup \Omega_*^{\varepsilon_0}$ we distinguish an elastic-dielectric part $\Omega_e^{\varepsilon_0}$, the piezoelectric segments $\Omega_z^{\varepsilon_0}$ and the electrodes $\Omega_*^{\alpha, \varepsilon_0} \subset \Omega_*^{\varepsilon_0}$, $\alpha = 1, 2$, being generated by periodically repeated copies of the reference cell Y components, see Fig. 5. Using (65) with the constants given in Tab. 2, the electric potential wave (the voltage) is imposed at $\Omega_*^{2, \varepsilon_0}$. To adhere with finite size electrodes, the unfolding brackets are employed: $\hat{x}_k = \varepsilon_0 \{x_k / \varepsilon_0\}_Y$ and (65) is employed with $\varphi^2(\hat{x}_1, \hat{x}_2, t)$, attaining piecewise constant values.

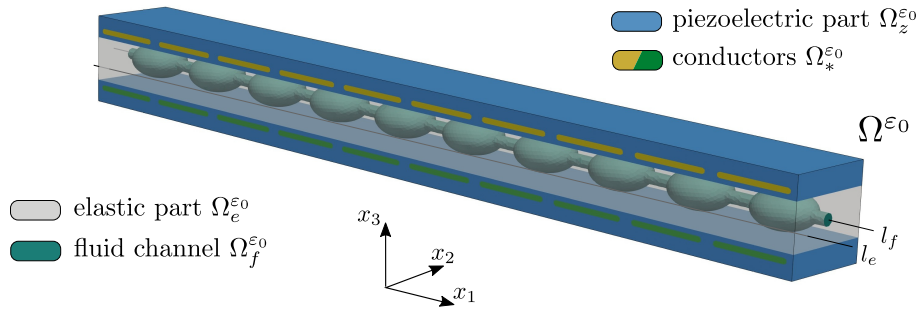


Figure 7: The geometry employed in the reference numerical simulation and two probe lines l_f , l_e along which the values in Section 5.3 are displayed.

To capture the model nonlinearity induced by imposing the REF-model equations in the “spatial” configuration deforming in time, we chose updating the geometry of the subdomains of $\Omega^{\varepsilon_0}(t)$ directly. In this way, we avoid any additional approximation as the one employed in the HOM-model, being based on the sensitivity analysis of the HOM-model effective coefficients. Instead, we implemented an iterative incremental computational algorithm with updates of the FE mesh used to discretize the subdomains on $\Omega^{\varepsilon_0}(t)$. In each iteration within a single time step, the nodes of the FE mesh are moved to new positions defined by the actual displacements. Such an iterative updating loop is repeated until the geometry updates are negligible, *i.e.* the iterations terminate when the norm of the displacement corrections is small enough.

5.3. Validation test

We consider the “pseudo 1D problem” imposed in the block specimen Ω , with the boundary conditions explained above, however, setting the fluid pressure to be zero on both the ends Γ_L and Γ_R of the specimen, $\bar{p} = 0$. Responses of both the REF- and HOM-models are computed for the actuation by $\bar{\varphi}^2 = 4 \cdot 10^5$ V according to (65) and the constants adjusted for the “1D” case, see Tab. 2, applied in 50 uniform time steps in the time interval $[0, 1]$ s. Note that $b_2 = 0$ so that $\varphi^2 = \varphi^2(x_1, t)$, whereby the above mentioned modification due to the finite size electrodes applies in the REF-model.

First we compare the linear HOM-model, for which the homogenized coefficients \mathbb{H}^0 are given by the non-perturbed configuration. Accordingly, the REF-model is used without updating the configuration, thus, solutions are computed on the fixed FE mesh. To provide a consistent responses corresponding to the finite heterogeneity captured by the REF-model, the macroscopic solutions of the HOM-model must be reconstructed at the microscopic level for a given finite scale ε^0 . The two-scale field reconstruction (sometimes called the “dowscaling”) is based on the decomposition formulae (37), details are discussed in [23]. The reconstructed pressure field p^{HOM, ε_0} and the displacement field u_1^{HOM, ε_0} together with the reference solutions p^{REF, ε_0} , u_1^{REF, ε_0} at selected time levels $t_k = 0.25, 0.5, 0.75$ s are compared in Fig. 9. Distributions of these fields are displayed along lines l_f , l_e parallel to the axis x_1 , see Fig. 7. The electric potential $\varphi^2(x_1, t_k)$ at the three selected times t_k is shown in Fig. 8.

In the second comparison, we consider nonlinear models so that the homogenized coefficients featuring the HOM-model are updated according to

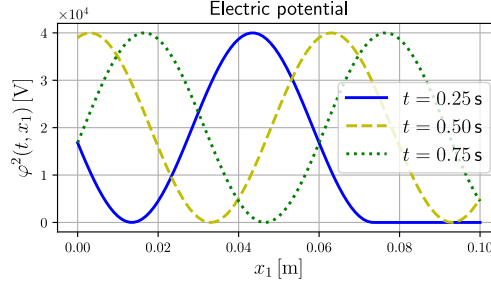


Figure 8: Spatial distribution of the control electric potential φ^2 at selected times t_k ; note the step-wise modification applies in the REF-model.

(55), whereby the macroscopic response is given by the algorithm described in Sec. 4.2.1. Accordingly, the REF-model responses are computed with the mesh updates in an iterative loop embedded in each time step, as described above. Results of this second comparison test are presented as in the first one; the reconstructed pressure and displacement fields with that obtained by the reference model are reported in Fig. 10. The reconstructed microscopic pressure, fluid velocity, and strain magnitude for a part of the specimen are depicted in Fig. 11.

To illustrate the effect of the model nonlinearity in the simulations, the cumulative fluxes through the middle face Γ_M computed as in (9), but with $w := w_1$ (fluxes aligned with the x_1 axis), are compared in Fig. 12 for the linear and nonlinear cases, *i.e.* without and with updating the homogenized coefficients using the approximation (55). Positive flux values mean the flow from Γ_L to Γ_R . While in linear case the flux oscillates around zero indicating no effective flux, in the nonlinear case, the pumping effect is obvious since the cumulative flux values increase with time, so that the fluid is transported from Γ_L to Γ_R .

5.4. Peristaltic pumping against natural flow

Now we examine the peristaltic pumping effect in the context the linear and nonlinear models. For this, modified data are considered. Given non-zero pressure \bar{p} on Γ_R , whereas $p = 0$ on Γ_L , the Darcy law induces a natural flow towards Γ_L . The pumping actuated by the induce peristaltic deformation wave running to the right should produce a net flux towards Γ_R , just in the opposite direction than the one of the natural flow. We choose $\bar{p} = 1$ kPa, and now put $\varepsilon^0 = 10^{-3}$, which means different material properties than those

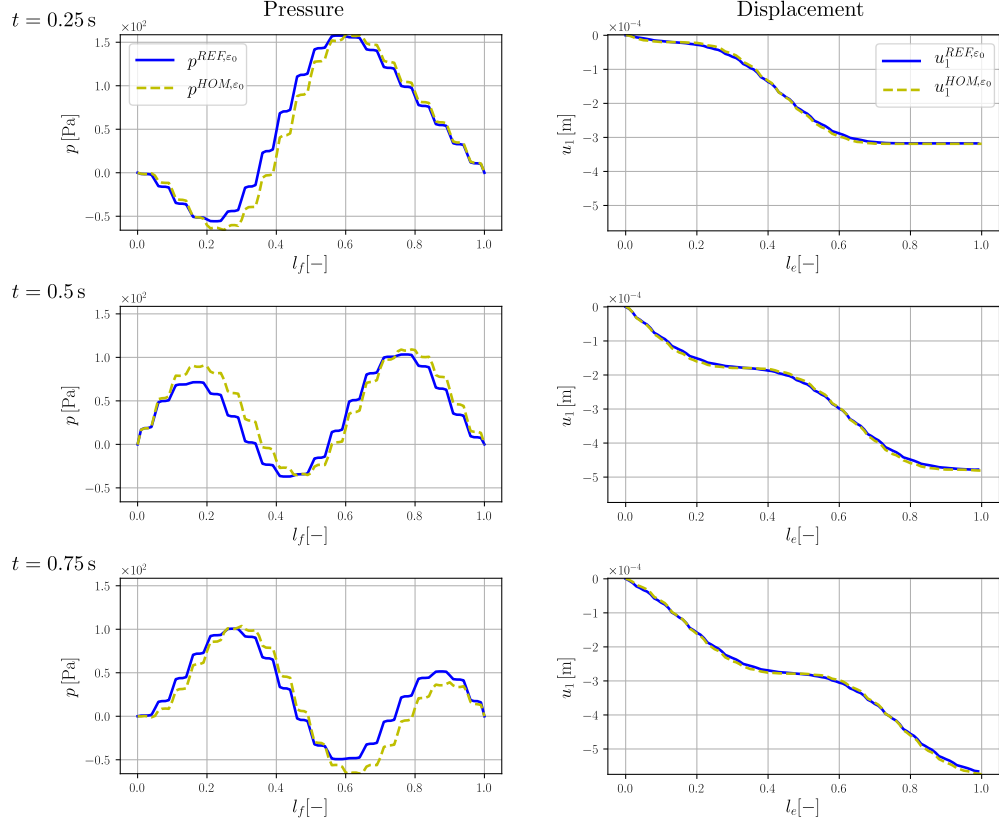


Figure 9: Comparison of homogenized and reference solutions – linear model.

considered in the above validation tests. The aim is to assess the influence of the electric voltage actuation $\bar{\varphi}^*$ on the amount of the fluid transported to the right Γ_R , see Fig. 13. For the electric potential $\bar{\varphi}^* = 0$ V, obviously, there is no peristalsis driven flow, the natural flow towards Γ_L due to the pressure gradient is obtained. By increasing $\bar{\varphi}^*$, the reverse flow can be achieved and for $\bar{\varphi}^* = 7 \cdot 10^4$ V a stable fluid transport due to the peristaltic pumping occurs.

The ability of the structure to transport fluid against pressure drop is strongly affected by the geometrical arrangement of the microstructure, especially by the shape of the fluid channel. This effect is illustrated in Fig. 14 where the cumulative fluxes for the “balloon \cap cylinder” fluid channel geometry and the simple cylindrical geometries are compared. As can be seen from

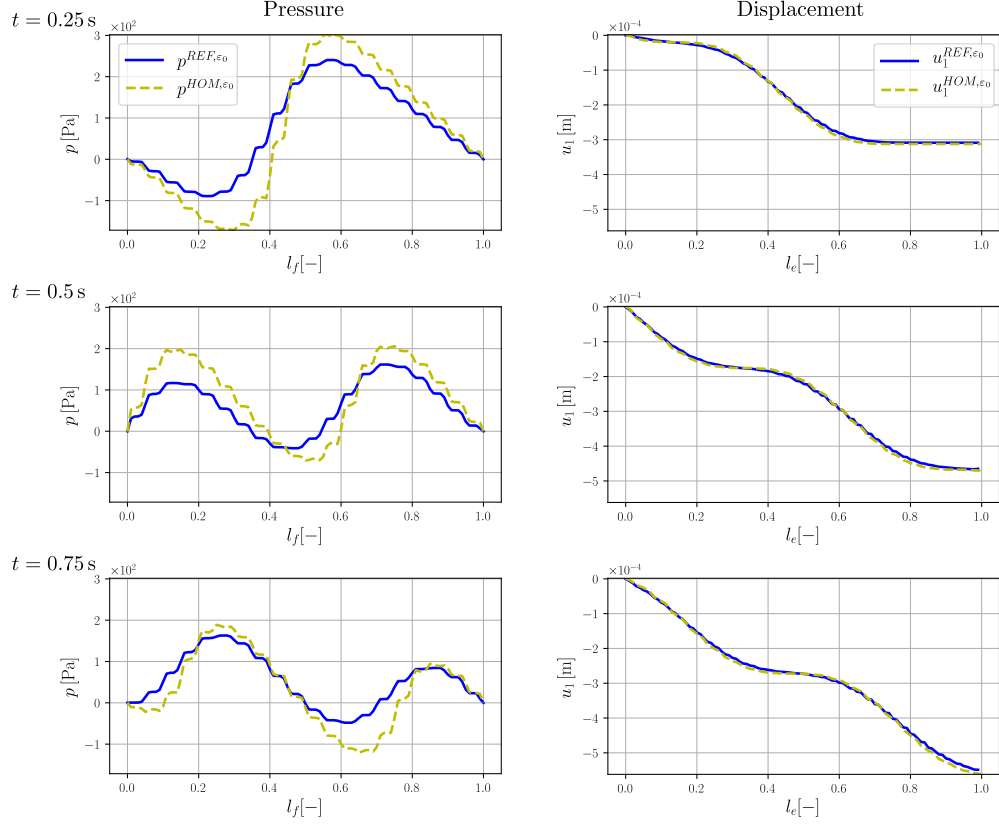


Figure 10: Comparison of homogenized and reference solutions – nonlinear model.

the figure, purely cylindrical fluid channels are not suitable for peristaltic fluid transport because cylinders with large diameters cannot be sufficiently throttled to eliminate reflux, while the smaller channels can only transport a limited amount of fluid for a given pressure gradient and electric potential.

5.5. Peristaltic flow in “2D” structure

In this section, we employ a modified periodic unit cell which allows for flows in the x_1 and x_2 directions, see Fig. 15/left, and the macroscopic sample of dimensions $0.1 \times 0.1 \times 0.0625$ m to which the boundary conditions depicted in Fig. 15/right are applied.

In order to demonstrate how the fluid transport through the structure can be controlled by the prescribed electric potential, we consider two distinct

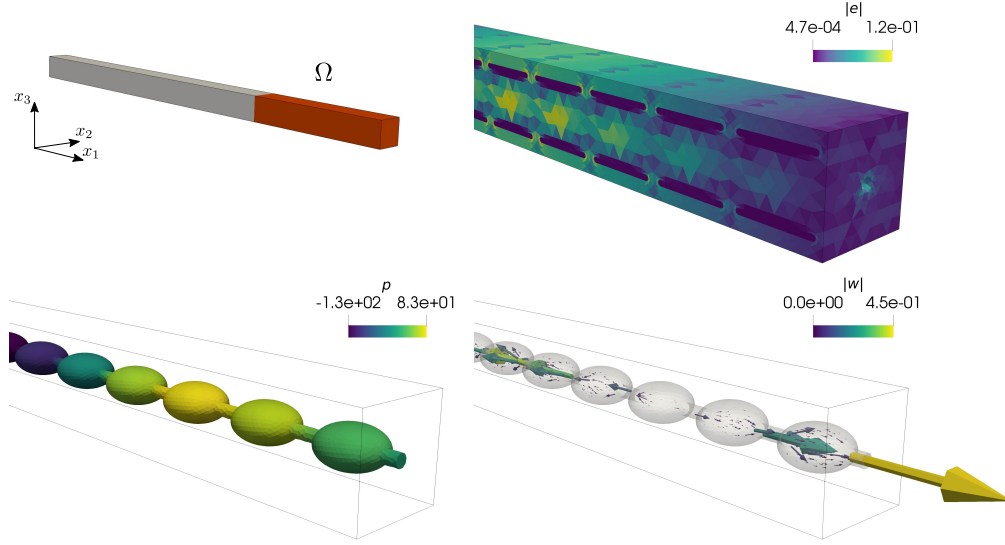


Figure 11: Reconstructed homogenized solution in the highlighted (red) part of Ω at time $t = 0.9$ s: strain magnitude $|\mathbf{e}(\mathbf{u}^{HOM, \varepsilon_0})|$ – top right, pressure p^{HOM, ε_0} – bottom left, velocity – bottom right.

functions φ^2 . In the first simulation, we employ the function $\varphi^2 = \varphi_I^2(x_1, t)$ identical to that used in Sec. 5.3 while the second simulation is performed for non-zero $d = \pi/0.75$ and $b_2 = \pi/0.075$, the “case 2D” in Tab. 2, so that $\varphi^2 = \varphi_{II}^2(x_1, x_2, t)$. The comparison of the cumulative fluxes through the faces $\Gamma_N, \Gamma_F, \Gamma_L$ for φ_I^2 and φ_{II}^2 is shown in Fig. 16.

The time evolution of the macroscopic pressure and velocity fields at simulation time levels $t_k = 0.14, 0.28, 0.42, 0.56$ s for the prescribed electric potential φ_I^2 is depicted in Fig. 17.

6. Conclusion

The presented work summarizes our research efforts aimed towards developing efficient computational tools to simulate behaviour of “smart porous” materials controllable by electric field which are designed to transport fluids using the principle of the peristaltic deformation. In particular, using the homogenization of the linearized fluid-structure interaction problem, we derived a model of electroactive porous material. The considered periodic composite structure involves piezoelectric actuators which provide a time-and-space

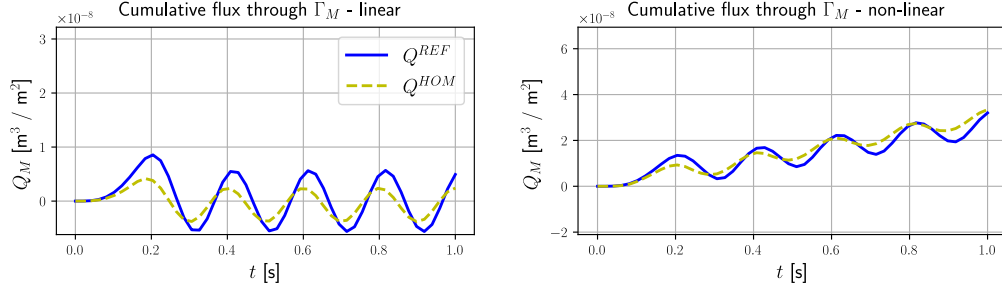


Figure 12: Cumulative flux through the internal faces Γ_M : linear model – left, nonlinear model – right.

control handle to induce a desired deformation wave. In this respect, the homogenized model (HOM-model) should be used for a given scale $\varepsilon_0 > 0$, *i.e.* a given size of the representative periodic cell $\varepsilon_0 Y$, since it is featured by the strong heterogeneity associated with the scaled material parameters of the micromodel. The HOM-model was validated by means of the DNS of the heterogeneous structure response taken as “the reference” (REF-model). As expected, the response of the homogenized medium provides a good approximation for the deformation field, while the approximation of the pressure is worse, in general. However, it should be noted, that, because of different treatment of the electrode (equipotential) segments, the prescribed control – the electric potential wave, is not quite the same for both the reference and the HOM-model, so that the comparison is rather affected by the control wave length. In our validations, to see the fluid transport effect, we had to keep the wave rather short compared to the number of the considered microstructure periods.

As confirmed by numerical studies, to achieve the desired pumping effect of the homogenized continuum, it is necessary to account for the nonlinearity associated with deformation-dependent microconfigurations and, hence, respecting deformation-dependent effective properties of the homogenized material. For this, the sensitivity analysis approach has been applied which leads to a computationally efficient numerical scheme for solving the nonlinear problem.

The main advantage of the derived homogenized model is the reduction of computational complexity. The reference computation with the FE mesh constituted by 20 periodic cells leads to a linear system with more than 300000 degrees of freedom, which must be solved in several iterations in each

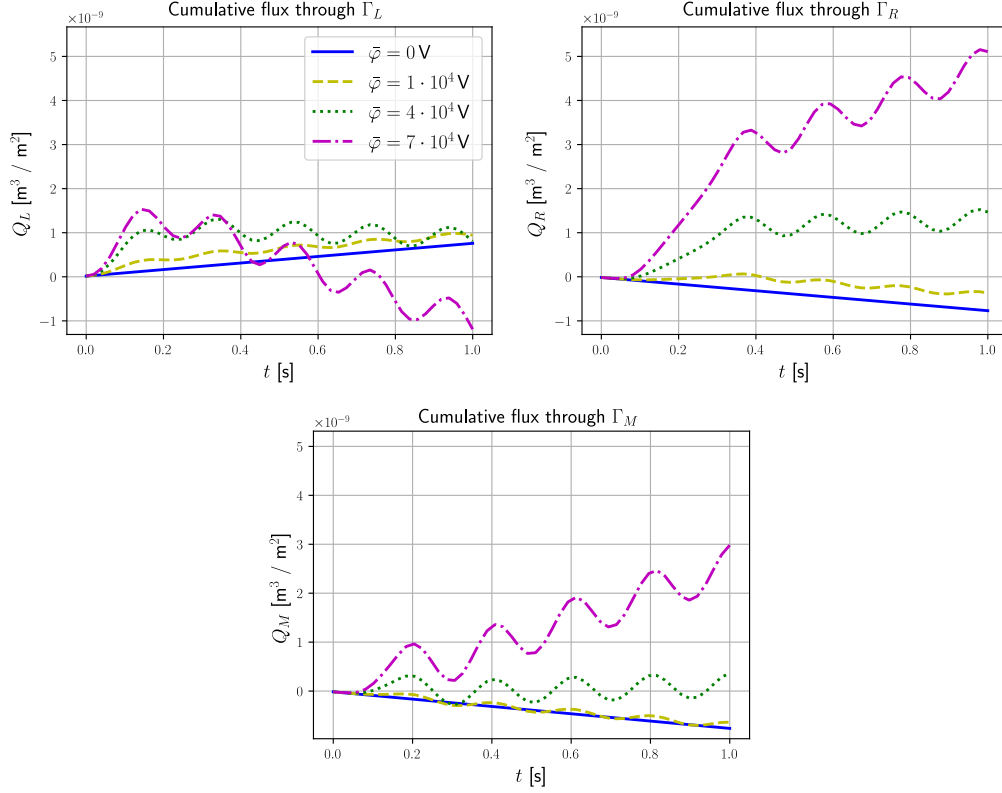


Figure 13: Cumulative flux through faces Γ_L , Γ_R , and Γ_M for various $\bar{\varphi}^*$.

time step. The solution of 50 time steps takes approximately 2 hours on a personal computer (10 core Intel i9 processor, 64GiB RAM). The two-scale calculation includes solving several microscopic subproblems, evaluating homogenized coefficients, and calculations at the macroscopic scale using a time stepping iterative algorithm. With a FE mesh consisting of ≈ 16000 tetrahedral elements and ≈ 3000 nodes at the microscopic level, the calculation time for all microscopic subproblems takes approximately half a minute. It can only be done once for a given microstructure and ε_0 . The macroscopic solution involving 50 time steps is obtained in less than 5 minutes including the two-scale field reconstructions, which is usually the most time consuming task in the whole calculation process. The efficiency of the proposed homogenization approach is obvious when comparing this short time (5 minutes) to the 2 hours required by the DNS of the heterogeneous structure.

The two-scale piezoelectric model respecting the geometrical nonlinear-

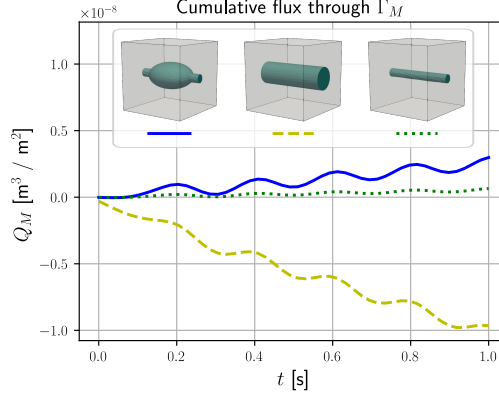


Figure 14: Cumulative flux through face Γ_M for three different fluid channel shapes, $\bar{\varphi}^* = 7 \cdot 10^4$ V.

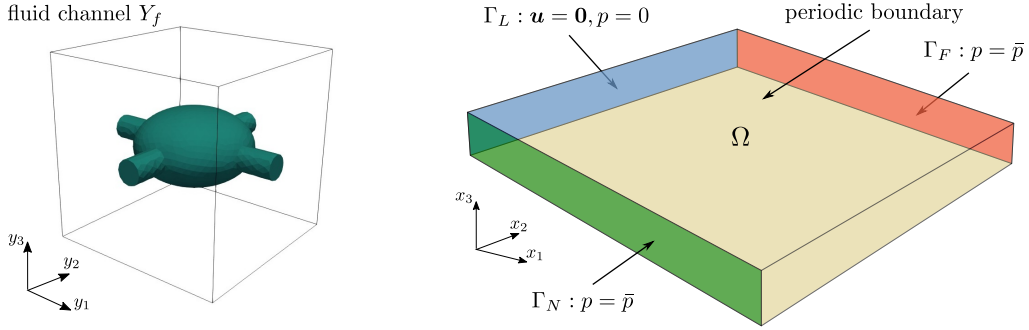


Figure 15: Microscopic periodic cell Y (left) and macroscopic domain Ω with an illustration of the applied boundary conditions (right).

ity seems to be an effective tool for simulating peristaltic flows in porous piezoelectric structures. Further studies and model refinement are envisaged towards using the acoustic wave energy for the fluid transport, in analogy with the “acoustic streaming” phenomenon. For this, the influence of the flow dynamics and respecting of all the inertia related phenomena will be important for higher frequencies of the voltage actuation through the piezoelectric actuators.

Acknowledgement. The research has been supported by the grant project GA 21-16406S of the Czech Science Foundation.

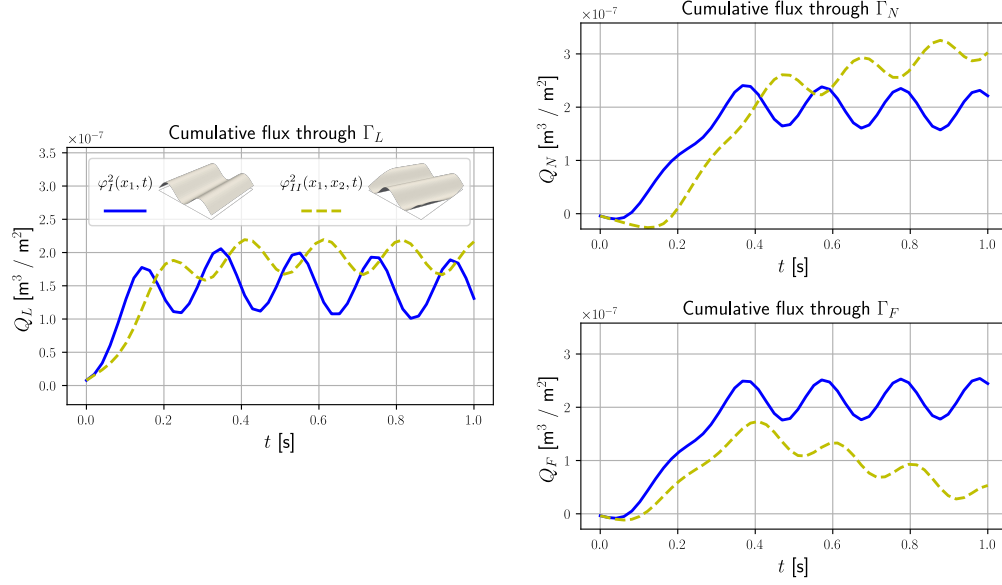


Figure 16: Cumulative fluxes through faces Γ_L , Γ_N , Γ_F for the electric potential given by φ_I^2 and φ_{II}^2 .

Appendix A: Sensitivity analysis of PZ-poroelastic coefficients

The sensitivity analysis of the homogenized coefficients is based on the so-called “design velocity method” of the shape sensitivity which is well known in the Structural Optimization. A “flux” of material points $y \in Y$ is given in terms of a differentiable and Y -periodic vector field $\vec{\mathcal{V}}(y)$, such that $z_i(y, \tau) = y_i + \tau \mathcal{V}_i(y)$, $y \in Y$, $i = 1, 2$, where τ is the “time-like” variable describes the perturbed position of $y \in Y$. We use the notion of the following derivatives: $\delta(\cdot)$ is the total (*material*) derivative, $\delta_\tau(\cdot)$ is the partial (*local*) derivative w.r.t. τ . These derivatives are computed as the directional derivatives in the direction of $\vec{\mathcal{V}}(y)$, $y \in Y$.

Preliminary results on the shape sensitivity

We shall use some particular results of the domain method of the shape sensitivity analysis which relies on the convection velocity field $\vec{\mathcal{V}}$. Auxiliary

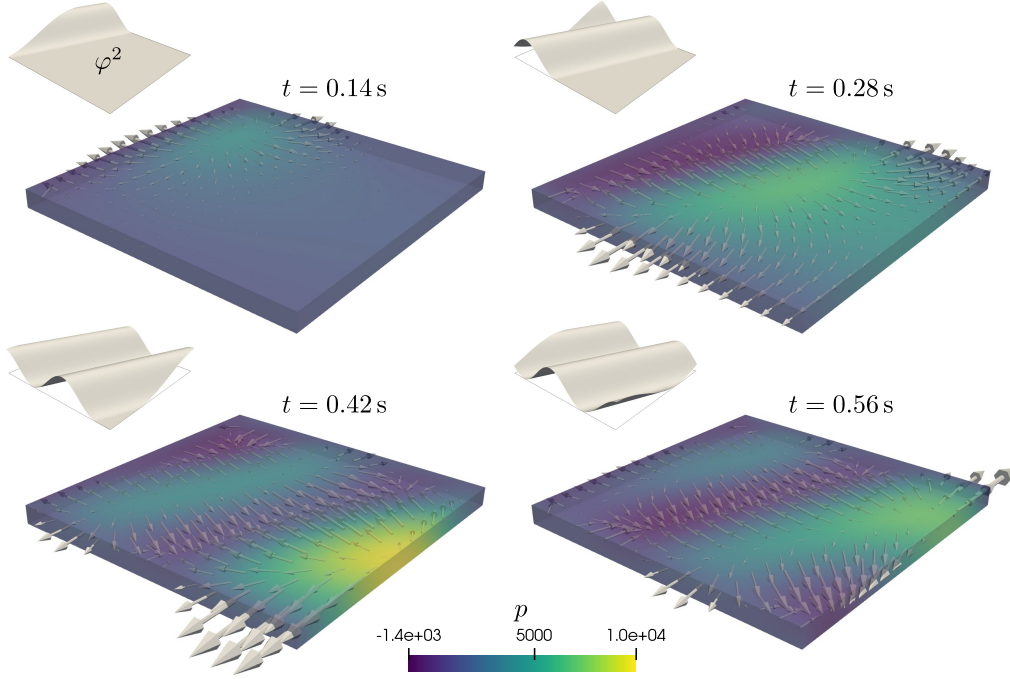


Figure 17: Macroscopic pressure and velocity fields at times $t_k = 0.14, 0.28, 0.42, 0.56$ s, $\varphi^2 = \varphi_{II}^2$.

results. Using (43),

$$\begin{aligned}
\delta_\tau |Y_d| &= \int_{Y_d} \nabla_y \cdot \vec{v} = \int_{\partial Y_d} \vec{v} \cdot \mathbf{n} , \\
\delta_\tau \phi_c &= |Y|^{-1} (\delta_\tau |Y_c| - \phi_c \delta_\tau |Y|) , \\
\delta_\tau \oint_{\Gamma_c} \mathbf{v} \cdot \mathbf{n}^{[c]} &= -\delta_\tau \oint_{Y_m} \nabla_y \cdot \mathbf{v} \\
&= \oint_{Y_m} \partial_i^y \mathcal{V}_k \partial_k^y v_i - \oint_{Y_m} \nabla_y \cdot \mathbf{v} \nabla_y \cdot \vec{v} + |Y|^{-1} \delta_\tau |Y| \oint_{Y_m} \nabla_y \cdot \mathbf{v} .
\end{aligned} \tag{66}$$

Note that $\delta_\tau |Y| = 0$ when \vec{v} is Y -periodic.

For the bilinear forms involved in the local problems, the following sensi-

tivity expressions hold:

$$\begin{aligned} \delta_\tau a_Y^{m*}(\mathbf{u}, \mathbf{v}) &= \oint_{Y_m \cup Y_*} D_{irks} \left(\delta_{rj} \delta_{sl} \nabla_y \cdot \vec{\mathcal{V}} - \delta_{jr} \partial_s^y \mathcal{V}_l - \delta_{ls} \partial_r^y \mathcal{V}_j \right) e_{kl}^y(\mathbf{u}) e_{ij}^y(\mathbf{v}) \\ &\quad - a_Y^{m*}(\mathbf{u}, \mathbf{v}) \oint_Y \nabla_y \cdot \vec{\mathcal{V}}, \end{aligned} \quad (67)$$

$$\begin{aligned} \delta_\tau d_Y^m(\varphi, \psi) &= \oint_{Y_m} d_{rs} \left(\delta_{ri} \delta_{sk} \nabla_y \cdot \vec{\mathcal{V}} - \delta_{ks} \partial_r^y \mathcal{V}_i - \delta_{ir} \partial_s^y \mathcal{V}_k \right) \partial_k^y \varphi \partial_i^y \psi \\ &\quad - d_Y^m(\varphi, \psi) \oint_Y \nabla_y \cdot \vec{\mathcal{V}}, \end{aligned} \quad (68)$$

$$\begin{aligned} \delta_\tau g_Y^m(\mathbf{u}, \psi) &= \oint_{Y_m} g_{jks} \left(\delta_{ij} \delta_{sl} \nabla_y \cdot \vec{\mathcal{V}} - \delta_{ij} \partial_s^y \mathcal{V}_l - \delta_{sl} \partial_j^y \mathcal{V}_i \right) e_{kl}^y(\mathbf{u}) \partial_i^y \psi \\ &\quad - g_Y^m(\mathbf{u}, \psi) \oint_Y \nabla_y \cdot \vec{\mathcal{V}}, \end{aligned} \quad (69)$$

We shall use the following notation:

$$\Xi^{ij} = \boldsymbol{\omega}^{ij} + \mathbf{\Pi}^{ij}, \text{ so that } \delta \Xi^{ij} = \delta \boldsymbol{\omega}^{ij} + \delta_\tau \mathbf{\Pi}^{ij}. \quad (70)$$

Differentiation of the microproblems

Using the above introduced notation, the following differentiated equations will be employed: Differentiated problem (39), for any $\mathbf{v} \in \mathbf{H}_\#^1(Y_{m*})$ and $\psi \in H_{\#0*}^1(Y_m)$, yields

$$\begin{aligned} a_Y^{m*}(\delta \boldsymbol{\omega}^{ij} + \delta_\tau \mathbf{\Pi}^{ij}, \mathbf{v}) - g_Y^m(\mathbf{v}, \delta \hat{\eta}^{ij}) &= -\delta_\tau a_Y^{m*}(\boldsymbol{\omega}^{ij} + \mathbf{\Pi}^{ij}, \mathbf{v}) + \delta_\tau g_Y^m(\mathbf{v}, \hat{\eta}^{ij}), \\ g_Y^m(\delta \boldsymbol{\omega}^{ij} + \delta_\tau \mathbf{\Pi}^{ij}, \psi) + d_Y^m(\delta \hat{\eta}^{ij}, \psi) &= -\delta_\tau g_Y^m(\boldsymbol{\omega}^{ij} + \mathbf{\Pi}^{ij}, \psi) - \delta_\tau d_Y^m(\hat{\eta}^{ij}, \psi). \end{aligned} \quad (71)$$

Differentiated problem (40), for any $\mathbf{v} \in \mathbf{H}_\#^1(Y_{m*})$ and $\psi \in H_{\#0*}^1(Y_m)$, yields

$$\begin{aligned} a_Y^{m*}(\delta \boldsymbol{\omega}^P, \mathbf{v}) - g_Y^m(\mathbf{v}, \delta \hat{\eta}^P) &= -\delta_\tau \oint_{\Gamma_c} \mathbf{v} \cdot \mathbf{n}^{[c]} dS_y - \delta_\tau a_Y^{m*}(\boldsymbol{\omega}^P, \mathbf{v}) + \delta_\tau g_Y^m(\mathbf{v}, \hat{\eta}^P), \\ g_Y^m(\delta \boldsymbol{\omega}^P, \psi) + d_Y^m(\delta \hat{\eta}^P, \psi) &= -\delta_\tau g_Y^m(\boldsymbol{\omega}^P, \psi) - \delta_\tau d_Y^m(\hat{\eta}^P, \psi). \end{aligned} \quad (72)$$

Differentiated problem (41), for any $\mathbf{v} \in \mathbf{H}_{\#}^1(Y_{m*})$ and $\psi \in H_{\#0*}^1(Y_m)$, yields

$$\begin{aligned} a_Y^{m*}(\delta\boldsymbol{\omega}^\rho, \mathbf{v}) - g_Y^m(\mathbf{v}, \delta\hat{\eta}^\rho) &= -\delta_\tau a_Y^{m*}(\boldsymbol{\omega}^\rho, \mathbf{v}) + \delta_\tau g_Y^m(\mathbf{v}, \hat{\eta}^\rho) , \\ g_Y^m(\delta\boldsymbol{\omega}^\rho, \psi) + d_Y^m(\delta\hat{\eta}^\rho, \psi) &= \delta_\tau \int_{\Gamma_{mc}} \psi \, dS_y - \delta_\tau g_Y^m(\boldsymbol{\omega}^\rho, \psi) - \delta_\tau d_Y^m(\hat{\eta}^\rho, \psi) . \end{aligned} \quad (73)$$

Differentiated problem (42), for any $\mathbf{v} \in \mathbf{H}_{\#}^1(Y_{m*})$ and $\psi \in H_{\#0*}^1(Y_m)$, yields

$$\begin{aligned} a_Y^{m*}(\delta\hat{\boldsymbol{\omega}}^k, \mathbf{v}) - g_Y^m(\mathbf{v}, \delta\hat{\varphi}^k) &= -\delta_\tau a_Y^{m*}(\hat{\boldsymbol{\omega}}^k, \mathbf{v}) + \delta_\tau g_Y^m(\mathbf{v}, \hat{\varphi}^k) , \\ g_Y^m(\delta\hat{\boldsymbol{\omega}}^k, \psi) + d_Y^m(\delta\hat{\varphi}^k, \psi) &= -\delta_\tau g_Y^m(\hat{\boldsymbol{\omega}}^k, \psi) - \delta_\tau d_Y^m(\hat{\varphi}^k, \psi) . \end{aligned} \quad (74)$$

Sensitivity of the HC

Using the identities of the local characteristic problems (39)-(42), and (31), and their differentiated forms derived above, we derive the sensitivity expressions of $\delta\mathbf{H} \circ \vec{\mathcal{V}}$ for all the homogenized coefficients (49) except of the permeability – for $\delta\mathbf{K}$ see [22]; note that the sensitivity expressions of the poroelastic coefficients treated in [22] cannot be used since, in our model, all theses are modified by the skeleton piezoelectricity.

Elasticity. Using (70), from (71) we get

$$\begin{aligned} \delta A_{kli}^H &= \delta_\tau a_Y^{m*}(\Xi^{ij}, \Xi^{kl}) + \delta_\tau d_Y^m(\hat{\eta}^{kl}, \hat{\eta}^{ij}) \\ &\quad + a_Y^{m*}(\delta\Xi^{ij}, \Xi^{kl}) + a_Y^{m*}(\Xi^{ij}, \delta\Xi^{kl}) + d_Y^m(\delta\eta^{kl}, \hat{\eta}^{ij}) + d_Y^m(\hat{\eta}^{kl}, \delta\eta^{ij}) , \end{aligned} \quad (75)$$

To eliminate $\delta\boldsymbol{\omega}^{ij}$ and $\delta\hat{\eta}^{ij}$, we use (39)₁ with $\mathbf{v} := \delta\boldsymbol{\omega}^{kl}$ and (71)₂ with substituted $\psi = \hat{\eta}^{ij}$,

$$\begin{aligned} a_Y^{m*}(\Xi^{ij}, \delta\boldsymbol{\omega}^{kl}) &= g_Y^m(\delta\boldsymbol{\omega}^{kl}, \hat{\eta}^{ij}) \\ &= -\delta_\tau g_Y^m(\Xi^{kl}, \hat{\eta}^{ij}) - \delta_\tau d_Y^m(\hat{\eta}^{kl}, \hat{\eta}^{ij}) - g_Y^m(\delta_\tau \boldsymbol{\Pi}^{kl}, \hat{\eta}^{ij}) - d_Y^m(\delta\hat{\eta}^{kl}, \hat{\eta}^{ij}) , \end{aligned} \quad (76)$$

hence (75) can be rewritten,

$$\begin{aligned} \delta A_{kli}^H &= \delta_\tau a_Y^{m*}(\Xi^{ij}, \Xi^{kl}) + \delta_\tau d_Y^m(\hat{\eta}^{kl}, \hat{\eta}^{ij}) \\ &\quad + a_Y^{m*}(\Xi^{ij}, \delta_\tau \boldsymbol{\Pi}^{kl}) + a_Y^{m*}(\delta_\tau \boldsymbol{\Pi}^{ij}, \Xi^{kl}) \\ &\quad - (\delta_\tau g_Y^m(\Xi^{kl}, \hat{\eta}^{ij}) + g_Y^m(\delta_\tau \boldsymbol{\Pi}^{kl}, \hat{\eta}^{ij}) - \delta_\tau d_Y^m(\hat{\eta}^{ij}, \hat{\eta}^{kl})) \\ &\quad - (\delta_\tau g_Y^m(\Xi^{ij}, \hat{\eta}^{kl}) + g_Y^m(\delta_\tau \boldsymbol{\Pi}^{ij}, \hat{\eta}^{kl}) - \delta_\tau d_Y^m(\hat{\eta}^{ij}, \hat{\eta}^{kl})) , \end{aligned} \quad (77)$$

so the cancellation due to $\delta_\tau d_Y^m(., .)$ symmetric term yields

$$\begin{aligned} \delta A_{kl ij}^H &= \delta_\tau a_Y^{m*}(\Xi^{ij}, \Xi^{kl}) - \delta_\tau d_Y^m(\hat{\eta}^{kl}, \hat{\eta}^{ij}) \\ &\quad + a_Y^{m*}(\Xi^{ij}, \delta_\tau \Pi^{kl}) + a_Y^{m*}(\delta_\tau \Pi^{ij}, \Xi^{kl}) \\ &\quad - (\delta_\tau g_Y^m(\Xi^{kl}, \hat{\eta}^{ij}) + \delta_\tau g_Y^m(\Xi^{ij}, \hat{\eta}^{kl}) + g_Y^m(\delta_\tau \Pi^{kl}, \hat{\eta}^{ij}) + g_Y^m(\delta_\tau \Pi^{ij}, \hat{\eta}^{kl})) , \end{aligned} \quad (78)$$

Biot modulus. Differentiation of (49)₃ yields

$$\begin{aligned} \delta M^H &= \gamma \delta_\tau \phi_c + \delta_\tau a_Y^{m*}(\omega^P, \omega^P) + \delta_\tau d_Y^m(\hat{\eta}^P, \hat{\eta}^P) \\ &\quad + 2a_Y^{m*}(\delta \omega^P, \omega^P) + 2d_Y^m(\delta \hat{\eta}^P, \hat{\eta}^P) . \end{aligned} \quad (79)$$

To eliminate expressions involving $\delta \omega^P$ and $\hat{\eta}^P$, we substitute $\delta \omega^P$ in (72)₁, and $\delta \hat{\eta}^P$ in (40)₂, so that

$$\begin{aligned} a_Y^{m*}(\delta \omega^P, \omega^P) - g_Y^m(\omega^P, \delta \hat{\eta}^P) &= -\delta_\tau \oint_{\Gamma_c} \omega^P \cdot \mathbf{n}^{[c]} - \delta_\tau a_Y^{m*}(\omega^P, \omega^P) \\ &\quad + \delta_\tau g_Y^m(\omega^P, \hat{\eta}^P) , \\ g_Y^m(\omega^P, \delta \hat{\eta}^P) + d_Y^m(\hat{\eta}^P, \delta \hat{\eta}^P) &= 0 , \end{aligned} \quad (80)$$

which upon summation yields

$$\begin{aligned} &a_Y^{m*}(\delta \omega^P, \omega^P) + d_Y^m(\delta \hat{\eta}^P, \hat{\eta}^P) \\ &= \delta_\tau g_Y^m(\omega^P, \hat{\eta}^P) - \delta_\tau a_Y^{m*}(\omega^P, \omega^P) - \delta_\tau \oint_{Y_c} \omega^P \cdot \mathbf{n}^{[c]} , \end{aligned} \quad (81)$$

hence

$$\begin{aligned} \delta M^H &= \gamma \delta_\tau \phi_c - 2\delta_\tau \oint_{\Gamma_c} \omega^P \cdot \mathbf{n}^{[c]} \\ &\quad + \delta_\tau d_Y^m(\hat{\eta}^P, \hat{\eta}^P) + 2\delta_\tau g_Y^m(\omega^P, \hat{\eta}^P) - \delta_\tau a_Y^{m*}(\omega^P, \omega^P) . \end{aligned} \quad (82)$$

Note that the sensitivity of the boundary integral in (82) can be expressed in terms of volume integrals according to (66).

Biot coupling coefficients. Differentiation of (49)₂ yields

$$\delta B_{ij}^H = \delta_\tau \phi_c \delta_{ij} - \delta_\tau \oint_{Y_m} \nabla_y \cdot \omega^{ij} - \oint_{Y_m} \nabla_y \cdot \delta \omega^{ij} . \quad (83)$$

where, due to (43), the last integral can be expressed using (40)₁ with substituted $\mathbf{v} := \delta\omega^{ij}$,

$$\oint_{Y_m} \nabla_y \cdot \delta\omega^{ij} = a_Y^{m*}(\omega^P, \delta\omega^{ij}) - g_Y^m(\delta\omega^{ij}, \hat{\eta}^P) . \quad (84)$$

Using (72)₁ with substituted $\mathbf{v} := \omega^P$ we get

$$\begin{aligned} a_Y^{m*}(\omega^P, \delta\omega^{ij}) &= -a_Y^{m*}(\omega^P, \delta_\tau \Pi^{ij}) - \delta_\tau a_Y^{m*}(\omega^P, \Xi^{ij}) \\ &\quad + g_Y^m(\omega^P, \delta\hat{\eta}^{ij}) + \delta_\tau g_Y^m(\omega^P, \hat{\eta}^{ij}) . \end{aligned} \quad (85)$$

From (40)₂ and (71)₂ we obtain

$$\begin{aligned} g_Y^m(\omega^P, \delta\hat{\eta}^{ij}) &= -d_Y^m(\hat{\eta}^P, \delta\hat{\eta}^{ij}) \\ &= \delta_\tau d_Y^m(\hat{\eta}^P, \hat{\eta}^{ij}) + \delta_\tau g_Y^m(\Xi^{ij}, \hat{\eta}^P) + g_Y^m(\delta\Xi^{ij}, \hat{\eta}^P) , \end{aligned} \quad (86)$$

where $\delta\Xi^{ij}$ is expressed using (70). By the consequence, upon substituting (85) and (86) into (84), the second r.h.s. integral in (84) cancels and we get

$$\begin{aligned} \oint_{Y_m} \nabla_y \cdot \delta\omega^{ij} &= \delta_\tau g_Y^m(\omega^P, \hat{\eta}^{ij}) - \delta_\tau a_Y^{m*}(\omega^P, \Xi^{ij}) - a_Y^{m*}(\omega^P, \delta_\tau \Pi^{ij}) \\ &\quad + \delta_\tau g_Y^m(\Xi^{ij}, \hat{\eta}^P) + g_Y^m(\delta_\tau \Pi^{ij}, \hat{\eta}^P) + \delta_\tau d_Y^m(\hat{\eta}^P, \hat{\eta}^{ij}) , \end{aligned} \quad (87)$$

so that the sensitivity (83) can be rewritten, as follows

$$\begin{aligned} \delta B_{ij}^H &= \delta_\tau \phi_c \delta_{ij} - \delta_\tau \oint_{Y_m} \nabla_y \cdot \omega^{ij} + a_Y^{m*}(\omega^P, \delta_\tau \Pi^{ij}) + \delta_\tau a_Y^{m*}(\omega^P, \Xi^{ij}) \\ &\quad - (\delta_\tau g_Y^m(\omega^P, \hat{\eta}^{ij}) + \delta_\tau g_Y^m(\Xi^{ij}, \hat{\eta}^P) + g_Y^m(\delta_\tau \Pi^{ij}, \hat{\eta}^P) + \delta_\tau d_Y^m(\hat{\eta}^P, \hat{\eta}^{ij})) . \end{aligned} \quad (88)$$

Stress-voltage coupling coefficients. Differentiation of (49)₄ yields

$$\begin{aligned} \delta H_{ij}^k &= a_Y^{m*}(\delta\hat{\omega}^k, \Pi^{ij}) - g_Y^m(\Pi^{ij}, \delta\hat{\varphi}^k) \\ &\quad + a_Y^{m*}(\hat{\omega}^k, \delta_\tau \Pi^{ij}) - g_Y^m(\delta_\tau \Pi^{ij}, \hat{\varphi}^k) + \delta_\tau a_Y^{m*}(\hat{\omega}^k, \Pi^{ij}) - \delta_\tau g_Y^m(\Pi^{ij}, \hat{\varphi}^k) . \end{aligned} \quad (89)$$

To eliminate the presence of $\delta\hat{\omega}^k$ and $\delta\hat{\varphi}^k$, we employ (39) with substitutions $\mathbf{v} := \delta\hat{\omega}^k$ and $\psi := \delta\hat{\varphi}^k$, which yields

$$\begin{aligned} a_Y^{m*}(\delta\hat{\omega}^k, \Pi^{ij}) &= g_Y^m(\delta\hat{\omega}^k, \hat{\eta}^{ij}) - a_Y^{m*}(\delta\hat{\omega}^k, \omega^{ij}) , \\ -g_Y^m(\Pi^{ij}, \delta\hat{\varphi}^k) &= g_Y^m(\omega^{ij}, \delta\hat{\varphi}^k) + d_Y^m(\hat{\eta}^{ij}, \delta\hat{\varphi}^k) . \end{aligned} \quad (90)$$

Further, we employ (74) with $\mathbf{v} := \boldsymbol{\omega}^{ij}$ and $\psi := \hat{\eta}^{ij}$ to substitute the terms involving $\delta\hat{\boldsymbol{\omega}}^k$ in (90)₁, hence

$$\begin{aligned} a_Y^{m*}(\delta\hat{\boldsymbol{\omega}}^k, \boldsymbol{\Pi}^{ij}) &= -g_Y^m(\boldsymbol{\omega}^{ij}, \delta\hat{\varphi}^k) + \delta_\tau a_Y^{m*}(\hat{\boldsymbol{\omega}}^k, \boldsymbol{\omega}^{ij}) - \delta_\tau g_Y^m(\boldsymbol{\omega}^{ij}, \hat{\boldsymbol{\omega}}^k) \\ &\quad - d_Y^m(\delta\hat{\varphi}^k, \hat{\eta}^{ij}) - \delta_\tau g_Y^m(\hat{\boldsymbol{\omega}}^k, \hat{\eta}^{ij}) - \delta_\tau d_Y^m(\hat{\varphi}^k, \hat{\eta}^{ij}) . \end{aligned} \quad (91)$$

The terms containing $\delta\hat{\varphi}^k$ can be replaced using (90)₂, so that

$$\begin{aligned} a_Y^{m*}(\delta\hat{\boldsymbol{\omega}}^k, \boldsymbol{\Pi}^{ij}) - g_Y^m(\boldsymbol{\Pi}^{ij}, \delta\hat{\varphi}^k) &= \\ \delta_\tau a_Y^{m*}(\hat{\boldsymbol{\omega}}^k, \boldsymbol{\omega}^{ij}) - \delta_\tau g_Y^m(\boldsymbol{\omega}^{ij}, \hat{\boldsymbol{\omega}}^k) - \delta_\tau g_Y^m(\hat{\boldsymbol{\omega}}^k, \hat{\eta}^{ij}) - \delta_\tau d_Y^m(\hat{\varphi}^k, \hat{\eta}^{ij}) . \end{aligned} \quad (92)$$

Finally, the sensitivity (89) can be evaluated by

$$\begin{aligned} \delta H_{ij}^k &= a_Y^{m*}(\hat{\boldsymbol{\omega}}^k, \delta_\tau \boldsymbol{\Pi}^{ij}) - g_Y^m(\delta_\tau \boldsymbol{\Pi}^{ij}, \hat{\varphi}^k) - \delta_\tau g_Y^m(\hat{\boldsymbol{\omega}}^k, \hat{\eta}^{ij}) - \delta_\tau d_Y^m(\hat{\varphi}^k, \hat{\eta}^{ij}) \\ &\quad + \delta_\tau a_Y^{m*}(\hat{\boldsymbol{\omega}}^k, \boldsymbol{\omega}^{ij} + \boldsymbol{\Pi}^{ij}) - \delta_\tau g_Y^m(\boldsymbol{\omega}^{ij} + \boldsymbol{\Pi}^{ij}, \hat{\varphi}^k) . \end{aligned} \quad (93)$$

Pressure-voltage coupling coefficients. Differentiation of (49)₇ yields

$$\delta Z^k = - \oint_{\Gamma_c} \delta\hat{\boldsymbol{\omega}}^k \cdot \mathbf{n}^{[c]} - \delta_\tau \oint_{\Gamma_c} \hat{\boldsymbol{\omega}}^k \cdot \mathbf{n}^{[c]} . \quad (94)$$

To eliminate $\delta\hat{\boldsymbol{\omega}}^k$, first substitute $\mathbf{v} := \delta\hat{\boldsymbol{\omega}}^k$ in (40)₁, then employ (74) with $\mathbf{v} := \boldsymbol{\omega}^P$ and $\psi := \hat{\eta}^P$. Thus, we get

$$\begin{aligned} - \oint_{\Gamma_c} \delta\hat{\boldsymbol{\omega}}^k \cdot \mathbf{n}^{[c]} &= a_Y^{m*}(\boldsymbol{\omega}^P, \delta\hat{\boldsymbol{\omega}}^k) - g_Y^m(\delta\hat{\boldsymbol{\omega}}^k, \hat{\eta}^P) \\ &= g_Y^m(\delta\hat{\varphi}^k, +) \delta_\tau g_Y^m(\boldsymbol{\omega}^P, \hat{\varphi}^k) - \delta_\tau a_Y^{m*}(\hat{\boldsymbol{\omega}}^k, \boldsymbol{\omega}^P) \\ &\quad + d_Y^m(\delta\hat{\varphi}^k, \hat{\eta}^P) + \delta_\tau g_Y^m(\hat{\boldsymbol{\omega}}^k, \hat{\eta}^P) + \delta_\tau d_Y^m(\hat{\varphi}^k, \hat{\eta}^P) . \end{aligned} \quad (95)$$

Above the terms involving $\delta\hat{\varphi}^k$ due to (40). The final sensitivity reads

$$\begin{aligned} \delta Z^k &= \delta_\tau g_Y^m(\boldsymbol{\omega}^P, \hat{\varphi}^k) - \delta_\tau a_Y^{m*}(\hat{\boldsymbol{\omega}}^k, \boldsymbol{\omega}^P) \\ &\quad \delta_\tau g_Y^m(\hat{\boldsymbol{\omega}}^k, \hat{\eta}^P) + \delta_\tau d_Y^m(\hat{\varphi}^k, \hat{\eta}^P) - \delta_\tau \oint_{\Gamma_c} \hat{\boldsymbol{\omega}}^k \cdot \mathbf{n}^{[c]} . \end{aligned} \quad (96)$$

where the sensitivity of the boundary integral is evaluated according to (66).

Appendix B: Perturbed integral forms

For the linearization scheme (63)-(64) employed in the Newton method, see Section 4, we need the first order approximation (62) of the integrals involving the perturbed homogenized coefficients. Below we present analogical expressions to (62) for all the integrals involved in the weak formulation (50).

$$\begin{aligned}
& \int_{\Omega} \mathbf{e}(\mathbf{v}) : \tilde{\mathbb{A}}(\mathbf{e}(\mathbf{u}), p, \varphi) \mathbf{e}(\mathbf{u}) = \int_{\Omega} \mathbf{e}(\mathbf{v}) : (\mathbb{A}^0 + \partial_e \mathbb{A}^0 \circ \mathbf{e}(\mathbf{u}) + \partial_p \mathbb{A}^0 \circ p + \partial_{\varphi} \mathbb{A}^0 \circ \varphi) \mathbf{e}(\mathbf{u}) \\
& \approx \int_{\Omega} \mathbf{e}(\mathbf{v}) : (\mathbb{A}^0 + \partial_e \mathbb{A}^0 \circ (\mathbf{e}(\bar{\mathbf{u}}) + \mathbf{e}(\delta \mathbf{u})) + \partial_p \mathbb{A}^0 \circ (\bar{p} + \delta p) + \partial_{\varphi} \mathbb{A}^0 \circ (\bar{\varphi} + \delta \varphi)) \mathbf{e}(\bar{\mathbf{u}}) \\
& \quad + \int_{\Omega} \mathbf{e}(\mathbf{v}) : (\mathbb{A}^0 + \partial_e \mathbb{A}^0 \circ \mathbf{e}(\bar{\mathbf{u}}) + \partial_p \mathbb{A}^0 \circ \bar{p} + \partial_{\varphi} \mathbb{A}^0 \circ \bar{\varphi}) \mathbf{e}(\delta \mathbf{u}) .
\end{aligned}$$

$$\begin{aligned}
& \int_{\Omega} p \tilde{\mathbf{B}}(\mathbf{e}(\mathbf{u}), p, \varphi) : \mathbf{e}(\mathbf{v}) = \int_{\Omega} p (\mathbf{B}^0 + \partial_e \mathbf{B}^0 \circ \mathbf{e}(\mathbf{u}) + \partial_p \mathbf{B}^0 \circ p + \partial_{\varphi} \mathbf{B}^0 \circ \varphi) : \mathbf{e}(\mathbf{v}) \\
& \approx \int_{\Omega} \bar{p} (\mathbf{B}^0 + \partial_e \mathbf{B}^0 \circ (\mathbf{e}(\bar{\mathbf{u}}) + \mathbf{e}(\delta \mathbf{u})) + \partial_p \mathbf{B}^0 \circ (\bar{p} + \delta p) + \partial_{\varphi} \mathbf{B}^0 \circ (\bar{\varphi} + \delta \varphi)) : \mathbf{e}(\mathbf{v}) \\
& \quad + \int_{\Omega} \delta p (\mathbf{B}^0 + \partial_e \mathbf{B}^0 \circ \mathbf{e}(\bar{\mathbf{u}}) + \partial_p \mathbf{B}^0 \circ \bar{p} + \partial_{\varphi} \mathbf{B}^0 \circ \bar{\varphi}) : \mathbf{e}(\mathbf{v}) .
\end{aligned}$$

$$\begin{aligned}
& \int_{\Omega} q \tilde{\mathbf{B}}(\mathbf{e}(\mathbf{u}), p, \varphi) : \mathbf{e}(\dot{\mathbf{u}}) = \int_{\Omega} q (\mathbf{B}^0 + \partial_e \mathbf{B}^0 \circ \mathbf{e}(\mathbf{u}) + \partial_p \mathbf{B}^0 \circ p + \partial_{\varphi} \mathbf{B}^0 \circ \varphi) : \mathbf{e}(\dot{\mathbf{u}}) \\
& \approx \int_{\Omega} q (\mathbf{B}^0 + \partial_e \mathbf{B}^0 \circ (\mathbf{e}(\bar{\mathbf{u}}) + \mathbf{e}(\delta \mathbf{u})) + \partial_p \mathbf{B}^0 \circ (\bar{p} + \delta p) + \partial_{\varphi} \mathbf{B}^0 \circ (\bar{\varphi} + \delta \varphi)) : \mathbf{e}(\dot{\mathbf{u}}) \\
& \quad + \int_{\Omega} q (\mathbf{B}^0 + \partial_e \mathbf{B}^0 \circ \mathbf{e}(\bar{\mathbf{u}}) + \partial_p \mathbf{B}^0 \circ \bar{p} + \partial_{\varphi} \mathbf{B}^0 \circ \bar{\varphi}) : \mathbf{e}(\delta \dot{\mathbf{u}})
\end{aligned}$$

$$\begin{aligned}
& \int_{\Omega} q \tilde{M}(\mathbf{e}(\mathbf{u}), p, \varphi) \dot{p} = \int_{\Omega} q (M^0 + \partial_e M^0 \circ \mathbf{e}(\mathbf{u}) + \partial_p M^0 \circ p + \partial_{\varphi} M^0 \circ \varphi) \dot{p} \\
& \approx \int_{\Omega} q (M^0 + \partial_e M^0 \circ (\mathbf{e}(\bar{\mathbf{u}}) + \mathbf{e}(\delta \mathbf{u})) + \partial_p M^0 \circ (\bar{p} + \delta p) + \partial_{\varphi} M^0 \circ (\bar{\varphi} + \delta \varphi)) \dot{p} \\
& \quad + \int_{\Omega} q (M^0 + \partial_e M^0 \circ \mathbf{e}(\bar{\mathbf{u}}) + \partial_p M^0 \circ \bar{p} + \partial_{\varphi} M^0 \circ \bar{\varphi}) \delta \dot{p}
\end{aligned}$$

$$\begin{aligned}
& \int_{\Omega} \varphi \tilde{\mathbf{H}}(\mathbf{e}(\mathbf{u}), p, \varphi) : \mathbf{e}(\mathbf{v}) = \int_{\Omega} \varphi (\mathbf{H}^0 + \partial_e \mathbf{H}^0 \circ \mathbf{e}(\mathbf{u}) + \partial_p \mathbf{H}^0 \circ p + \partial_{\varphi} \mathbf{H}^0 \circ \varphi) : \mathbf{e}(\mathbf{v}) \\
& \approx \int_{\Omega} \bar{\varphi} (\mathbf{H}^0 + \partial_e \mathbf{H}^0 \circ (\mathbf{e}(\bar{\mathbf{u}}) + \mathbf{e}(\delta \mathbf{u})) + \partial_p \mathbf{H}^0 \circ (\bar{p} + \delta p) + \partial_{\varphi} \mathbf{H}^0 \circ (\bar{\varphi} + \delta \varphi)) : \mathbf{e}(\mathbf{v}) \\
& + \int_{\Omega} \delta \varphi (\mathbf{H}^0 + \partial_e \mathbf{H}^0 \circ \mathbf{e}(\bar{\mathbf{u}}) + \partial_p \mathbf{H}^0 \circ \bar{p} + \partial_{\varphi} \mathbf{H}^0 \circ \bar{\varphi}) : \mathbf{e}(\mathbf{v}) .
\end{aligned}$$

$$\begin{aligned}
& \int_{\Omega} q \tilde{Z}(\mathbf{e}(\mathbf{u}), p, \varphi) \dot{\varphi} = \int_{\Omega} q (Z^0 + \partial_e Z^0 \circ \mathbf{e}(\mathbf{u}) + \partial_p Z^0 \circ p + \partial_{\varphi} Z^0 \circ \varphi) \dot{\varphi} \\
& \approx \int_{\Omega} q (Z^0 + \partial_e Z^0 \circ (\mathbf{e}(\bar{\mathbf{u}}) + \mathbf{e}(\delta \mathbf{u})) + \partial_p Z^0 \circ (\bar{p} + \delta p) + \partial_{\varphi} Z^0 \circ (\bar{\varphi} + \delta \varphi)) \dot{\varphi} \\
& + \int_{\Omega} q (Z^0 + \partial_e Z^0 \circ \mathbf{e}(\bar{\mathbf{u}}) + \partial_p Z^0 \circ \bar{p} + \partial_{\varphi} Z^0 \circ \bar{\varphi}) \delta \dot{\varphi}
\end{aligned}$$

$$\begin{aligned}
& \int_{\Omega} \nabla q \cdot \tilde{\mathbf{K}}(\mathbf{e}(\mathbf{u}), p) \nabla p = \int_{\Omega} \nabla q \cdot (\mathbf{K}^0 + \partial_e \mathbf{K}^0 \circ \mathbf{e}(\mathbf{u}) + \partial_p \mathbf{K}^0 \circ p + \partial_{\varphi} \mathbf{K}^0 \circ \varphi) \nabla p \\
& \approx \int_{\Omega} \nabla q \cdot (\mathbf{K}^0 + \partial_e \mathbf{K}^0 \circ (\mathbf{e}(\bar{\mathbf{u}}) + \mathbf{e}(\delta \mathbf{u})) + \partial_p \mathbf{K}^0 \circ (\bar{p} + \delta p) + \partial_{\varphi} \mathbf{K}^0 \circ (\bar{\varphi} + \delta \varphi)) \nabla \bar{p} \\
& + \int_{\Omega} \nabla q \cdot (\mathbf{K}^0 + \partial_e \mathbf{K}^0 \circ \mathbf{e}(\bar{\mathbf{u}}) + \partial_p \mathbf{K}^0 \circ \bar{p} + \partial_{\varphi} \mathbf{K}^0 \circ \bar{\varphi}) \nabla \delta p
\end{aligned}$$

Note that we can put $\delta \varphi = 0$ since φ is considered as a given variable.

- [1] Allaire, G., 1992. Homogenization of the unsteady Stokes equations in porous media, in: *Progress in Partial Differential Equations: Calculus of Variations, Applications*. volume 296 of *Pitman Research Notes in Mathematics Series*, pp. 109–123.
- [2] Ayuso, G.M., Friswell, M.I., Adhikari, S., Khodaparast, H.H., Berger, H., 2017. Homogenization of porous piezoelectric materials. *Int J Solids Struct* 113-114, 218–229. DOI:10.1016/j.ijsolstr.2017.03.003.
- [3] Carew, E.O., Pedley, T.J., 1997. An Active Membrane Model for Peristaltic Pumping: Part I—Periodic Activation Waves in an Infinite Tube. *J Biomech Eng* 119, 66–76. DOI:10.1115/1.2796066.

- [4] Chen, Y., Kadic, M., Wegener, M., 2021. Chiral triclinic metamaterial crystals supporting isotropic acoustical activity and isotropic chiral phonons. *Proc R Soc A* DOI:10.1098/rspa.2020.0764.
- [5] Chen, Z., Lyons, S., Qin, G., 2001. Derivation of the Forchheimer law via homogenization. *Transport Porous Med* 44, 325–335. DOI:10.1023/A:1010749114251.
- [6] Cimrman, R., Lukeš, V., Rohan, E., 2019. Multiscale finite element calculations in python using sfepy. *Lect Notes Pure Appl* 45, 18971921. DOI:10.1007/s10444-019-09666-0.
- [7] Cioranescu, D., Damlamian, A., Griso, G., 2008. The periodic unfolding method in homogenization. *Siam J Math Anal* 40, 1585–1620. DOI:10.1137/080713148.
- [8] Cioranescu, D., Donato, P., 1999. An introduction to homogenization. Number 17 in *Oxford Lecture Series in Mathematics and its Applications*, Oxford University Press, Oxford.
- [9] Clopeau, T., Ferrín, J., Gilbert, R., Mikelić, A., 2001. Homogenizing the acoustic properties of the seabed, Part II. *Math Comput Model* 33, 821–841. DOI:10.1016/S0895-7177(00)00283-1.
- [10] Fung, Y.C., Yih, C.S., 1968. Peristaltic Transport. *J Appl Mech* 35, 669–675. DOI:10.1115/1.3601290.
- [11] Herrera-Valencia, E.E., Rey, A.D., 2014. Actuation of flexoelectric membranes in viscoelastic fluids with applications to outer hair cells. *Philos T R Soc A* 372, 20130369. DOI:10.1098/rsta.2013.0369.
- [12] Hornung, U., 1997. Homogenization and porous media. Springer, Berlin.
- [13] Iyer, S., Venkatesh, T., 2014. Electromechanical response of (3-0, 3-1) particulate, fibrous, and porous piezoelectric composites with anisotropic constituents: A model based on the homogenization method. *Int J Solids Struct* 51, 1221 – 1234. DOI:10.1016/j.ijsolstr.2013.12.008.
- [14] Koutsawa, Y., Belouettar, S., Makradi, A., Nasser, H., 2010. Sensitivities of effective properties computed using micromechanics differential

- schemes and high-order taylor series: Application to piezo-polymer composites. *Mech Res Commun* 37, 489–494. DOI:10.1016/j.mechrescom.2010.06.001.
- [15] Lukeš, V., Rohan, E., 2022. Homogenization of large deforming fluid-saturated porous structures. *Comput Math Appl* 110, 40–63. DOI:10.1016/j.camwa.2022.01.036.
 - [16] Maiti, S., Misra, J.C., 2011. Peristaltic flow of a fluid in a porous channel: A study having relevance to flow of bile within ducts in a pathological state. *Int J Eng Sci* 49, 950–966. DOI:10.1016/j.ijengsci.2011.05.006.
 - [17] Mawassy, N., Reda, H., Ganghoffer, J., Eremeyev, V., Lakiss, H., 2021. A variational approach of homogenization of piezoelectric composites towards piezoelectric and flexoelectric effective media. *Int J Eng Sci* 158, 103410. DOI:10.1016/j.ijengsci.2020.103410.
 - [18] Miara, B., Rohan, E., Zidi, M., Labat, B., 2005. Piezomaterials for bone regeneration design—homogenization approach. *J Mech Phys Solids* 53, 2529–2556. DOI:10.1016/j.jmps.2005.05.006.
 - [19] Mikelic, A., Wheeler, M., 2012. On the interface law between a deformable porous medium containing a viscous fluid and an elastic body. *Math Models Meth Appl Sci* 22, 1–32. DOI:10.1142/S0218202512500315.
 - [20] Peszyńska, M., Trykozko, A., 2010. Forchheimer law in computational and experimental studies of flow through porous media at porescale and mesoscale. *Curr Adv Nonlin Anal Relat Top* 32, 463–482.
 - [21] Pozrikidis, C., 1987. A study of peristaltic flow. *J Fluid Mech* 180, 515–527. DOI:10.1017/S0022112087001939.
 - [22] Rohan, E., Lukeš, V., 2015. Modeling nonlinear phenomena in deforming fluid-saturated porous media using homogenization and sensitivity analysis concepts. *Appl Math Comput* 267, 583–595. DOI:10.1016/j.amc.2015.01.054.

- [23] Rohan, E., Lukeš, V., 2018. Homogenization of the fluid-saturated piezoelectric porous media. *Int J Solids Struct* 147, 110–125. DOI:10.1016/j.ijsolstr.2018.05.017.
- [24] Rohan, E., Miara, B., 2006. Homogenization and shape sensitivity of microstructures for design of piezoelectric bio-materials. *Mech Adv Mater Struc* 13, 473–485. DOI:10.1080/15376490600862848.
- [25] Rohan, E., Naili, S., 2020. Homogenization of the fluid-structure interaction in acoustics of porous media perfused by viscous fluid. *ZAMP-Z Angew Math Phys* 71, 137–164. DOI:10.1007/s00033-020-01361-1.
- [26] Sanchez-Palencia, E., 1980. Non-homogeneous media and vibration theory. Number 127 in *Lecture Notes in Physics*, Springer, Berlin.
- [27] Sandström, C., Larsson, F., Runesson, K., 2016. Homogenization of coupled flow and deformation in a porous material. *Comput Method Appl M* 308, 535–551. DOI:10.1016/j.cma.2016.05.021.
- [28] Sikavitsas, V.I., Temenoff, J.S., Mikos, A.G., 2001. Biomaterials and bone mechanotransduction. *Biomaterials* 22, 2581–2593. DOI:10.1016/S0142-9612(01)00002-3.
- [29] Viano, J., Ribeiro, C., Figueiredo, J., Rodríguez-Arós, A., 2016. A high order model for piezoelectric rods: An asymptotic approach. *Int J Solids Struct* 81, 294 – 310. DOI:10.1016/j.ijsolstr.2015.12.005.
- [30] Wiesmann, H.P., Hartig, M., Stratmann, U., Meyer, U., Joos, U., 2001. Electrical stimulation influences mineral formation of osteoblast-like cells in vitro. *BBA-Mol Cell Res* 1538, 28–37. DOI:10.1016/S0167-4889(00)00135-X.
- [31] Yvonnet, J., Chen, X., Sharma, P., 2020. Apparent flexoelectricity due to heterogeneous piezoelectricity. *J Appl Mech* 87. DOI:10.1115/1.4047981. 111003.